

AFIT/GA/ENY/93D-8

1

AD-A273 742


DTIC
ELECTE
DEC 16 1993
S A

**STEADY MOTIONS OF RIGID BODY SATELLITES
IN A CENTRAL GRAVITATIONAL FIELD**

THESIS
Cynthia Ann Provost
Captain, USAF

AFIT/GA/ENY/93D-8

93-30475


Approved for public release; distribution unlimited

98 12 15 08 1

The views expressed in this thesis are those of the author and do not reflect the official policy or position of the Department of Defense or the U. S. Government.

Accession For	
NTIS CRA&I	<input checked="" type="checkbox"/>
DTIC TAB	<input type="checkbox"/>
Unannounced	<input type="checkbox"/>
Justification	
By	
Distribution /	
Availability Codes	
Dist	Avail and/or Special
A-1	

DTIC QUALITY INSPECTED 1

AFIT/GA/ENY/93D-8

**STEADY MOTIONS OF RIGID BODY SATELLITES
IN A CENTRAL GRAVITATIONAL FIELD**

THESIS

**Presented to the Faculty of the Graduate School of Engineering
of the Air Force Institute of Technology
Air University
In Partial Fulfillment of the
Requirements for the Degree of
Master of Science in Astronautical Engineering**

**Cynthia Ann Provost, B.S. Aerospace Engineering
Captain, USAF**

December, 1993

Approved for public release; distribution unlimited

Preface

Celestial mechanics problems have motivated the development of both pure and applied mathematics since Newton's development of calculus. In fact, Newton used his calculus to formulate Kepler's laws of planetary motion and to show that a point mass may approximate a spherically symmetric body when considering gravitational attraction. Since then, generations of mathematicians have endeavored to improve the accuracy of the equations for planetary motion. In doing so, analytical methods, approximations, and gimmicks were formulated, greatly influencing instruction in mathematics. Although these nineteenth century mathematicians could have used the brute force method of literal numerical calculation, without the aid of modern-day computers the task would span lifetimes. Instead, particular tricks found useful in solving Kepler's laws were regarded as significant and subsequently added to the mathematician's box of tools. In retrospect it can be seen that the precomputer emphasis on analytical solutions was not entirely beneficial; many of these methods continue to be taught as an established mathematical means to an end, despite an era of sophisticated computers where approximate methods have little relevance (12:421,432), (6:85). On the other hand, analytical methods and their series- and closed-form solutions yield insight into the physical effects of specific parameters and the relative strengths of various physical mechanisms. Only the most successful numerical computations provide physical insight.

This thesis explores the implications of a set of mathematical tricks employed for centuries by those investigating celestial mechanics. It appears that this is one instance in which an analytical method produced a satisfactory and meaningful result in the past but may have also hidden the existence of a great number of alternative solutions. However, the spurious nature of these numerical results indicates that we must not completely abandon our centuries-old mathematical tricks. The emergence of supercomputers has seemingly produced answers in minutes rather than lifetimes, but only slightly diminishes our reliance on mathematical approximations and analytical methods.

Cynthia Ann Provost

Acknowledgements

I would like to acknowledge the contributions of the following individuals and organizations toward the preparation of this thesis and the completion of the AFIT program:

Captain Christopher D. Hall, USAF, for his understanding, patience, encouragement, and assistance in his role as advisor.

Dr. Arje Nachman and the Air Force Office of Scientific Research (AFOSR/NM) for sponsoring this research.

The Ohio Supercomputer Center, for the much-appreciated use of their Cray.

The members of the 1989-1993 Astronautical Engineering and 1993 and 1994 Space Operations student sections at AFIT for their friendship and support.

Lieutenant Colonel T.S. Kelso, USAF, for his technical and administrative assistance, as well as his class instruction emphasizing the "big picture."

My husband, Rob, for his patience, love, and "pep talks" without which this project would never have been completed.

Cynthia Ann Provost

Table of Contents

	Page
Preface	ii
Acknowledgements	iii
List of Figures	vi
List of Tables	vii
Abstract	viii
 I. Introduction	 1
1.1 Background	1
1.2 Problem Definition	5
1.3 Scope	5
1.4 Assumptions	5
1.5 Method	6
1.6 Overview	6
 II. Literature Review	 8
2.1 Gravitational Effects	8
2.2 Other Spacecraft Torques	9
2.3 Stability	12
2.4 Advantages of Gravity-Gradient Stabilization	14
2.5 Disadvantages of Gravity-Gradient Stabilization	15
2.6 Equilibrium Orientations	15
2.7 Unique Ideas	17
2.8 Operations	18

	Page
III. System Dynamics	21
3.1 Introduction	21
3.2 Gravity-Gradient Development	21
3.3 A Gravity-Gradient Alternative	24
IV. Methodology	30
4.1 Model Description	30
4.2 Continuation Method	31
4.3 Utilizing AUTO86	33
4.4 Accuracy Testing	34
4.5 Procedure	34
V. Results	37
5.1 Introduction	37
5.2 Discussion of Results	37
5.3 Modifications to Improve AUTO	51
5.4 Additional Steps Toward Efficiency and Accuracy	53
5.5 Problems Encountered	54
VI. Conclusions	57
6.1 Summary	57
6.2 Operational Significance	57
6.3 Recommendations	59
Appendix A. AUTO Subroutines	61
Bibliography	74
Vita	78

List of Figures

Figure		Page
1.	Sketches of Gravity-Gradient Satellites	2
2.	A Great Circle Orbit	4
3.	A Non-Great Circle Orbit	4
4.	Spacecraft Torques	11
5.	Rigid Body Motion in a Gravitational Field	22
6.	Orbital Configuration	25
7.	The Satellite Model	29
8.	Spherical Coordinate System	36
9.	Graphical Representation of Table 1	38
10.	Complete Results of AUTO	39
11.	AUTO Results in Range 1	41
12.	Enlarged AUTO Results in Range 1	42
13.	AUTO Results in Range 2	43
14.	Additional AUTO Results in Ranges 2 and 3	45
15.	AUTO Results Refined By NEWT	46
16.	AUTO Results in Range 3	47
17.	AUTO Results in Range 3 - Enlarged View	48
18.	AUTO Results in Range 4	49
19.	AUTO Results in Range 5	50
20.	Non-Great Circle Orbit Equilibrium Orientations	52

List of Tables

Table		Page
1.	Relative Equilibria Illustrating Large Orientation Drifts	35
2.	Range Definitions	40

Abstract

Numerous studies have been conducted on equilibrium orientations of objects moving under the influence of a central gravitational field. The objects under investigation have had configurations ranging from spheres to cylinders to more complicated three-axis stabilized satellites. The results of many of these studies conclude that equilibrium conditions exist only when one of the principal axes coincides with the radius vector. Furthermore, these results assume that the center of force is located within the orbit plane, thereby tracing a great circle orbit. While these previous works have approximated the gravitational potential, this study examines relative equilibria obtained by retaining an exact expression for the potential of a spherical primary body, as shown in a recent paper by Wang, Maddocks, and Krishnaprasad. The exact dynamic equations for the motion of a finite rigid body in an inverse square gravitational force field are investigated. Only circular orbits for a specific satellite model consisting of six masses connected by three massless rigid rods are considered. The system dynamics are comprised of seven nonlinear equations, which were numerically solved on a Cray computer. The existence of equilibrium orientations which establish non-great circle orbits was verified and other interesting results were noted. The operational significance of these results was also examined.

STEADY MOTIONS OF RIGID BODY SATELLITES IN A CENTRAL GRAVITATIONAL FIELD

I. Introduction

1.1 Background

The study of motions due to an inverse square gravitational potential field has been explored for several centuries. Orbiting bodies investigated include point masses, spheres, cylinders, rods, ball-and-socket connected objects, and more complicated bodies with moving appendages and momentum wheels. Until recently, many of these studies have utilized approximate solutions to the equations of motion obtained with a spherical primary body. Typically the gravitational force and moment acting on the body of interest has been approximated with a binomial series expansion and the center of force is assumed to be located within the orbit plane. Using these approximations generally leads to a result in which equilibrium conditions exist only when one of the principal axes coincides with the radius vector. This type of orientation is known as a gravity-gradient attitude. The trajectory for these types of satellites is a great circle orbit.

A gravity-gradient-stabilized satellite utilizes the gravitational force of a massive primary body for stability. The gravitational torques tend to align the axis of minimum moment of inertia with the radius vector from the center of mass of the satellite to the center of mass of the primary body. Use of this stability method requires that the satellite have specific mass and inertia properties. The most common feature of many gravity-gradient stabilized satellites is the presence of long booms. Some sketches of several of these types of spacecraft are depicted in Figure 1.

A great circle orbit is one in which the radius vector from the center of mass of the primary body to the center of mass of the orbiting body traces out a disk. This type of orbit is depicted in Figure 2. Conversely, the radius vector of a non-great circle orbit traces out a cone, as seen in Figure 3. In other words, "the center of relative equilibrium

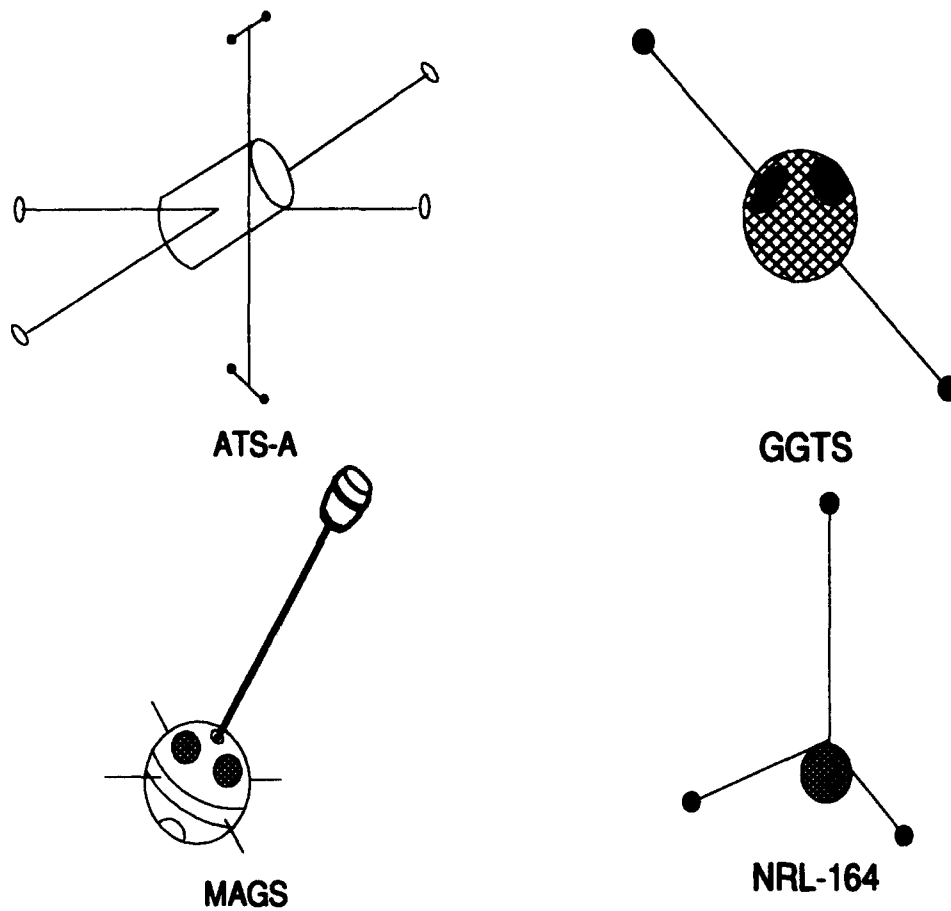


Figure 1. Sketches of Gravity-Gradient Satellites: Applications Technology Satellite-A (ATS-A) (24), Gravity-Gradient Test Satellite (GGTS) (24), Magnetically Anchored Gravity System (MAGS) (24), and the Naval Research Laboratory - 164 (NRL-164)(5).

rotation does not coincide with the center of the force field (41).” For a great circle orbit, it is obvious that the radius vector, \vec{r} , must be perpendicular to the angular velocity vector, $\vec{\omega}$, or $\vec{r} \cdot \vec{\omega} = 0$. Further analysis reveals that both $\vec{\omega}$ and \vec{r} must be aligned with principal axes. However, this restriction is not present in non-great circle orbits. In fact, it has been shown that although the offset from a great circle orbit is very small in certain circumstances, the attitude change associated with that offset can be quite significant (42).

In a recent paper by Wang, Maddocks, and Krishnaprasad (42) the concept of non-great circle orbits was explored. In their study, the Hamiltonian form of the exact dynamic equations for the motion of a finite rigid body in an inverse square gravitational force field was examined. The equations were found to have a noncanonical structure with the gravitational potential as one term. While previous works have approximated the gravitational potential, the Wang paper explores relative equilibria obtained by retaining an exact expression for the potential of a spherical primary body. The results of the Wang investigation were promising, yet not definitive. Using continuation techniques, numerous non-great circle orientations were discovered for an ideal, hypothetical structure consisting of 6 mass particles. Seven nonlinear algebraic equations were solved by successive application of Newton-Raphson iterations. However, several discontinuities in their results indicated potential bifurcation and limit points, implying the existence of distinct branches of equilibria. Additionally, the operational significance and feasibility of non-great circle orbit applications was not addressed. Furthermore, their results were based on a model which may not realistically represent a useful satellite in orbit.

If these additional questions were addressed, the results could have far-reaching effects on the design of earth-orbiting satellites. Different dynamical systems could then be analyzed with the exact potential, yielding previously unknown equilibrium orientations. Modifications to control systems which take into account newly-found stable orientations might achieve better performance and reduce consumption of on-orbit propellants used for station-keeping and attitude adjustment. Perhaps complex orbital missions could be achieved with less complex satellite configurations. Clearly, the results of (42) exhibit potential for future satellite design. However, further investigation is required to more closely examine the anomalies and significance of (42).

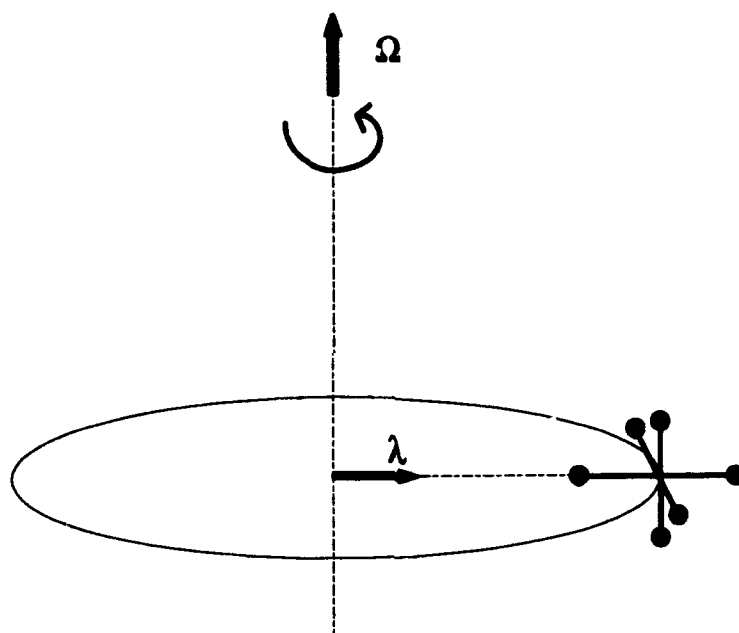


Figure 2. A Great Circle Orbit.

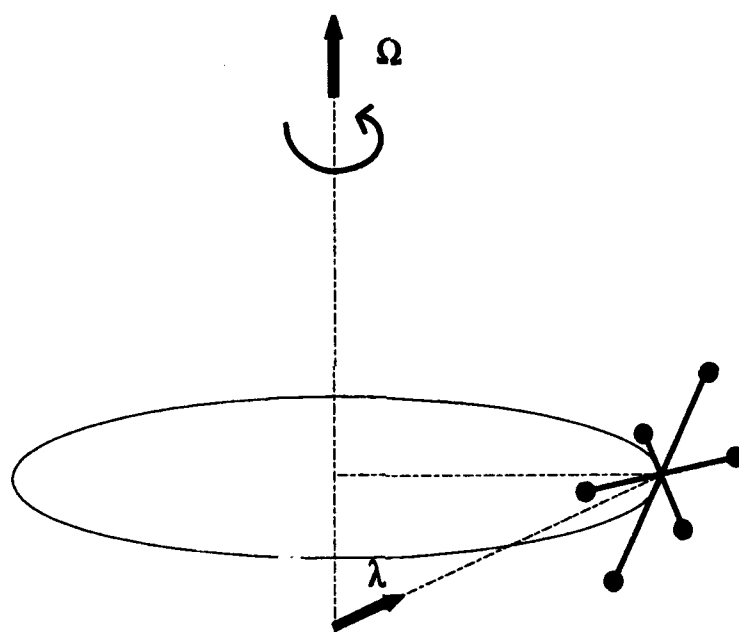


Figure 3. A Non-Great Circle Orbit.

1.2 Problem Definition

This investigation attempted to validate the findings of (42) and explore in greater detail the discontinuities present in their results. A computer program different from that used in (42), AUTO86 (4), was used to independently determine the existence of non-great circle relative equilibria for the six-particle model. AUTO86, referred to as AUTO for the remainder of this paper, is a continuation/bifurcation package, and its use was intended to facilitate the discovery of bifurcation points and successfully trace out branches of relative equilibria. AUTO was chosen because of recommendations from other users, the existence of several references and theses which utilized AUTO, and the software's availability. An objective examination of the operational utility of these relative equilibria was also conducted.

1.3 Scope

Although the original intent was to examine in further depth all the results obtained in (42), as well as utilize a more realistic satellite model, extensive difficulties in achieving valid and economically attainable results led to a restriction in scope. Consequently, this study is limited to the analysis of the exact six-particle molecule model used in (42). As described earlier, only relative equilibria for the molecule's motion due to an inverse-square gravitational field were sought. In the continuation method, only one parameter was varied in order to keep the Jacobian symmetric, thereby eliminating the need for a double precision eigenvalue solver and simplifying computations.

1.4 Assumptions

The dynamical system examined was assumed to have a circular orbit where the center of attraction may or may not be the center of the orbit. A restricted two-body approach was used by assuming the primary body is stationary. The solution obtained with the earth as a spherically symmetrical finite rigid body is identical to the solution obtained by treating it as a point mass. Thus, the earth was modelled here as a point mass. Consequently, harmonics associated with the oblateness of the earth are not considered. Although the very small size of the satellite model relative to its orbit radius could lead to

its treatment as a point mass, doing so would prevent analysis of satellite attitude. Thus the non-great circle relative equilibria of interest here were investigated by considering the finite extent of the orbiting rigid body.

1.5 Method

The dynamical equations were numerically analyzed on a computer, modelling the rigid body satellite as a simple molecular structure with unequal moments of inertia. First, the equations were coded and validated in double precision on a Sun SparcStation. Values of the function and the Jacobian were verified using the results of the program used in (42). The code was then incorporated into AUTO subroutines and tested for proper integration within the software. Subroutines were added to compute the necessary variables for accuracy testing. Insufficient accuracy was obtained using the Sun workstation, therefore the code was transferred to the Ohio Supercomputer Cray where double precision accuracy to 29 digits was possible (29). Initial equilibrium points were obtained from values depicted in Table 2 of (42). The AUTO code was run numerous times with different values for stepsizes, iterations, and tolerances to achieve results with sufficient accuracy. Hundreds of combinations were used in an intensive search for valid results. Apparent numerical instabilities caused several problems in obtaining data and excessive computer processing time. Several attempts at scaling and other modifications to AUTO were made to improve computer efficiency and accuracy. When this was accomplished, the results were compared to those found in (42). While the results of this project were not as conclusive as had been anticipated, some results of (42) were verified.

1.6 Overview

Following this introduction is a literature review which gives a synopsis of significant studies on relative equilibria of bodies moving under a gravitational field. Next, a development of the gravity-gradient orientation concept is presented in Chapter III. Correspondingly, a development of the theory on which this study is based is described. Chapter IV outlines the solution approach while in Chapter V the numerical results are analyzed and interpreted. Conclusions regarding the significance and operational applicability of

the concepts are contained in Chapter VI. Finally, recommendations for further study are provided.

II. Literature Review

In classical rigid-body dynamics, relative equilibria, a term attributed to Poincaré, are stationary rotations about the principal axes of inertia (36), (41). Although the subject of this report is relative equilibria of rigid body satellites, the concept parallels so closely with gravity-gradient satellites that a literature review of the latter serves as an excellent background for the former. Thus, this chapter primarily focusses on research, operations, and ideas pertaining to gravity-gradient torques and stabilization.

2.1 Gravitational Effects

According to Griffin, "planetary gravitational fields decrease with distance R from the center of the planet according to the Newtonian $1/R^2$ law," assuming higher order harmonics are neglected (6:293). Only the mass center of the spacecraft is in a true gravitationally-derived orbit. This explains why an orbiting object experiences a stronger attraction on its "lower" side than its "upper side." A spacecraft mass particle closer to the earth would move ahead of a mass particle farther away from earth's center if in a free orbit. If this differential force is applied to a body with unequal principal moments of inertia, a resulting torque tends to rotate the object, vertically aligning its minimum inertia or longest axis. Alternatively stated, "perturbations from the equilibrium produce a restoring torque toward the stable vertical position, causing a periodic oscillatory or 'librational' motion ...and internal elastic forces in the structure balance the orbital dynamic accelerations tending to separate masses orbiting at different altitudes (6:64-65,293)."

Several authors describe gravity-gradient torque in a similar manner. Satellites with unequal principal moments of inertia have torques acting upon them due to the gradient of the earth's gravitational field. According to (39), "these torques tend to align the axis of least moment of inertia with the local vertical. Therefore, in principle, the gravity-gradient torques can be used as the basis of a stabilization system for an earth-pointing satellite." Thomson states that "gravity torque tends to align the axis of minimum moment of inertia of a non-spinning body with the radius vector drawn from the center of Earth (38)." More specific descriptions of the vehicle orientation can be found in (41): "the angular velocity

lies along the principal axis of the body with the largest associated moment of inertia (minor axis of the ellipsoid of inertia), and the radius vector is aligned to the principal axis with the least associated moment of inertia (major axis of the ellipsoid of inertia)," and (17): "maintaining a fixed orientation with respect to a rotating reference frame established by the binormal, tangent, and principal normal of the orbital path."

The effects of gravity-gradient torques can be significant, depending on the distance from the center of the gravitational field and the shape of the orbiting body. For large vehicles such as a space station or space shuttle the magnitude may be $10^{-3}g$'s or more (6:64). According to (47), when considering gravitational, magnetic, solar radiation, aerodynamic, and cosmic dust disturbances, gravity-gradient torques are the most dominant torque over a large range of altitudes. Furthermore, the spacecraft yaw angle does not influence the gravity-gradient torque, since yaw represents rotation around the local vertical. The torque magnitude depends on the difference between principal moments of inertia. Therefore, cylindrical spacecraft are more affected than disk-shaped spacecraft (6:294).

2.2 Other Spacecraft Torques

To put the gravity-gradient concept into perspective, a brief discussion of a satellite's surrounding space environment is in order. The review will be limited to a description of various torques which affect bodies orbiting the earth.

A space vehicle orbiting the earth, or any other gravitational body, is subject to a number of disturbance torques. Although some have postulated that the gravitational gradient torque is the only external torque on the body (17), there are others. Torques due to aerodynamic loads, magnetic fields, solar wind and radiation, particle impingement, outgassing, and internal moving parts also affect a space vehicle.

Aerodynamic torque arises from the separation between the mass center and aerodynamic center of pressure (6:292). Momentum is transferred from atmospheric molecules to the surface of the space vehicle (13:250). This torque is also referred to as atmospheric resistance (30).

Magnetic torque affects the space vehicle while under the influence of the earth's magnetic field. Comparable to the alignment of a compass needle with the local magnetic field, components aboard the spacecraft which contribute to the vehicle's magnetic moment may similarly cause alignment with the earth's magnetic field. Consequently, careful relative orientation of current loops, magnets, and electronics is required by system designers to ensure the total magnetic moment of the vehicle is zero (6:295), (13:265).

Solar radiation pressure torque also contributes to the overall motion of a spacecraft. This torque, sometimes attributed to the solar wind (31:83), is independent of velocity or position while the spacecraft remains in sunlight, and acts perpendicular to the sun line (6:295). At altitudes above 1000 km, the space vehicle disturbance torque environment is usually dominated by solar radiation pressure (6:294). According to (49), solar radiation produces a transverse thermal gradient in deployed booms, causing them to bend away from the sun. The bending affects satellites by moving both the center of mass and the center of solar pressure, and changing the inertia dyadic which produces a change in gravity restoring-torque as well as dynamic effects due to rigidity.

Torques may also be caused by passage through meteor showers or a collision with debris. The impact of a meteoroid would impart a short impulse to the spacecraft (31:83). Additionally, the spacecraft itself is the cause of several disturbance torques. Deliberate or accidental effluent venting and internal torques resulting from a momentum exchange also cause disturbances. The internal torques may arise from the motion of antennas, solar arrays, instruments, scanners, deployable booms, and other appendages (6:296). Those appendages in turn would be subject to linear acceleration, centrifugal force, and Coriolis force (30).

A graphical representation of some of these torques can be found in Figure 4, which originated in (47) and was modified in (13:271). The figure presents a useful comparison of the magnitudes of some disturbance torques as a function of altitude. The torques are linear in the parameter shown, with the gravity-gradient linear limit being about 15°. Thus, the gravity-gradient torque for $\theta = 5^\circ$ may be obtained by taking the appropriate value from Figure 4 and multiplying by 5, where θ indicates the offset angle from the vertical.

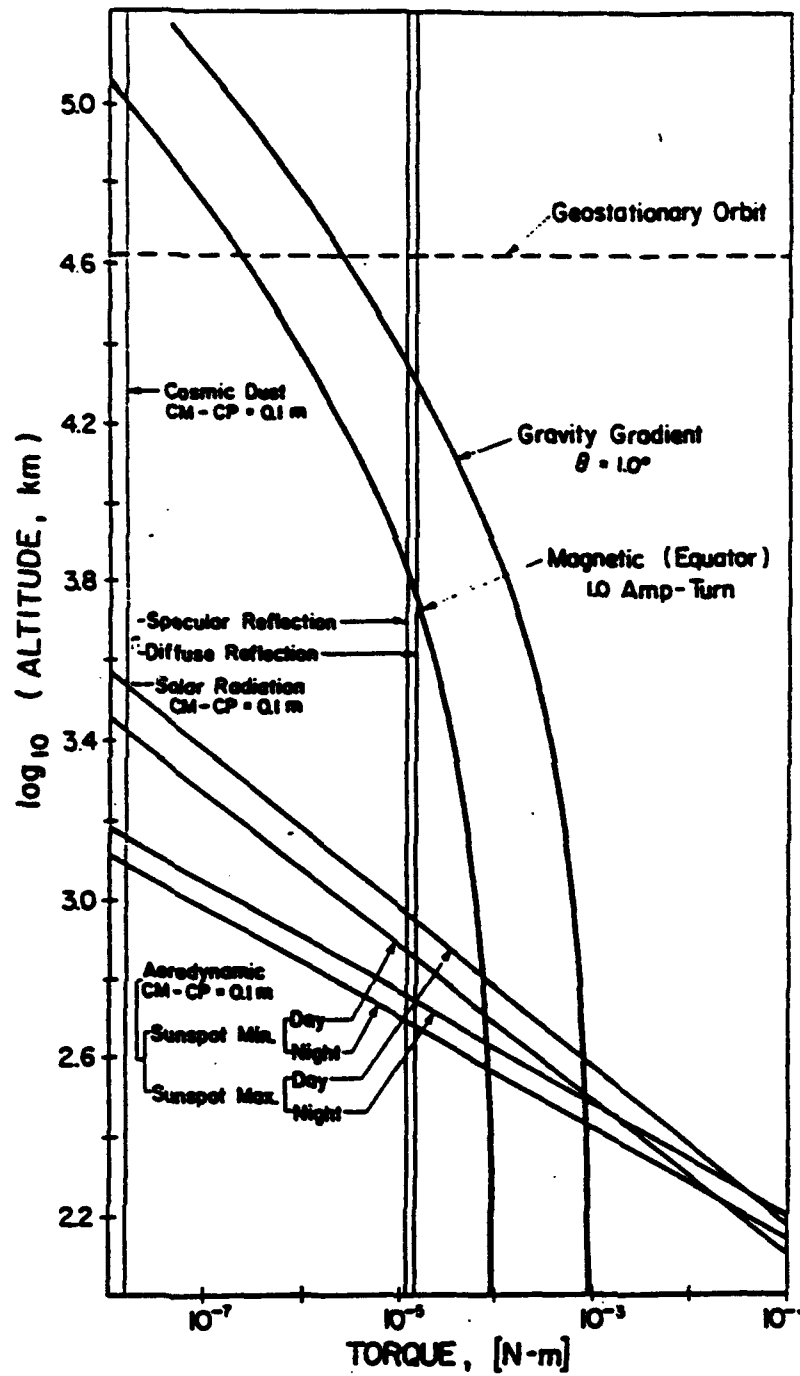


Figure 4. Comparison of several common torques on a typical spacecraft (47).

2.3 Stability

According to (24), the first published concept outlining a passive gravity-gradient control system is believed to exist in a U.S. patent issued to R.E. Roberson and J.V. Breakwell in 1956. This patent was only the first in a long line of technical reports concerning gravity-gradient stabilization systems. One aspect of gravity-gradient stabilization, and passive attitude control in general, is that it "takes advantage of basic physical principles and naturally occurring forces by designing the spacecraft so as to enhance the effect of one force while reducing others (6:297)." Dependable spacecraft stabilization permits electronic and optical tracking system performance to be optimized using more efficient antenna design and optimal orientation of onboard light sources or reflectors (18). In (1), the author reduces the problem of gravity-gradient stabilization to four major areas: 1) the reduction of tumbling 2) the extension of a boom or booms to achieve a large ratio of pitch- and roll-axis to yaw-axis moment of inertia 3) the damping of satellite librations to tolerable oscillations, and 4) controlling the satellite's boom position. Numerous authors have addressed these problems; several are described in this section.

In (19), the energy equation is used to determine the stability extrema of asymmetric satellites. Concurring with several other works, the author states that almost all satellites have a stable orientation. In particular, he addresses six dynamically distinct sets of equilibria, one of which is stable for any asymmetric rigid object in a circular orbit.

The problem of relative equilibria for gyrostats in a circular orbit is investigated by (48). In his paper, the author discusses a satellite composed of an arbitrary number of gyrostats interconnected by ball-and-socket joints. A gyrostat is a stabilizing device consisting of a small axisymmetric rotor, or momentum wheel, spinning about its axis of symmetry inside a platform. The rotor's spin does not affect the mass distribution and the inertia tensor of the gyrostat remains constant if the rotor and the platform are rigid bodies. A gyrostat is also referred to as a dual-spin satellite (31:264). First and second variations of the dynamic potential energy are used in (48) to obtain relative equilibrium positions and stability criteria.

The unpredictability of the direction of the pointing axis is described in (43). The author states: "All gravity-gradient stabilized satellites have a stable orientation which is either right side up or upside down. If after deployment the attitude and angular velocity are sufficient to cause tumbling, the final orientation may be upside down." The energy approach is used to predict capture or tumbling, thus indicating whether a turnover device is required (43).

The lack of inherent yaw stability present with gravity-gradient attitude control is briefly discussed in (6:300). Such a spacecraft is unconstrained and may rotate about its vertical axis. Consequently, large amplitude librations are sometimes observed which may be sufficient to invert the spacecraft. This anomalous behavior has been associated with the long-period resonances in the gravity-gradient boom when excited by thermal input, as described in (5) and (28:16).

In (38), the author discusses the potential stabilization of a particular type of spacecraft through the use of spin. The particular vehicle configuration, with its symmetric axis normal to the orbit plane, is apparently unstable when $I_2 < I_1$. I_1 and I_2 are the moments of inertia along the transverse and symmetric axes respectively. According to (38), the amount of spin required to stabilize the spacecraft depends on the angular velocity of the orbit radius and the ratio I_2/I_1 .

Presenting a general approach to the "rigorous nonlinear stability analysis of relative equilibria in Hamiltonian systems" was the author's intent in (36). In this paper, the author applied the reduced energy-momentum method to acquire an explicit and easily implementable criterion for nonlinear stability of relative equilibria. His method involves only the configuration variables and does not introduce Lagrange multipliers. The method also does not require explicit knowledge of momenta and momenta variations or the conserved quantities in the reduced space, also known as Casimirs (36).

Several other authors have examined the design of gravity-gradient stabilized spacecraft. Specifically, in (13:281-346), an excellent presentation on torques, stability, design and flight experience pertaining to gravitational forces is found. The stability conditions obtained through variational methods is the also the subject of (41). Additionally, the

effect of a variable gravitational force acting on a rod satellite is presented in (31:83). Three types of gravity-gradient stabilization configurations — traac, magnetic anchor, and hinged multibody — are discussed in (9).

While the gravitational torques present in orbit can provide a useful stabilizing force, additional measures are sometimes required to put the spacecraft in a proper gravity-gradient orientation from its deployment attitude, and also to minimize the naturally occurring libration. Although it is often required to position a satellite in orbit oriented in a specified direction, maintaining the specified attitude may be impeded due to perturbing torques (38). In (23), several methods for this type of stabilization are described. Magnetic stabilization can be used to assist the space vehicle in assuming its desired gravity-gradient attitude. The same can be accomplished using the previously mentioned boom deployment. Other methods include magnetic hysteresis rods, a damping spring with magnetic hysteresis rods, and magnetic hysteresis plus eddy-current damping.

In (39), "a passive three-axis stabilization system is described which relies solely on the gravity-gradient to provide both the damping and the restoring torques for a vertically-oriented satellite." Damping occurs through the energy dissipation of relative motion existing between the main spacecraft vehicle and an auxiliary body.

Exploring allowable attitude deviations due to given disturbances was the intent of the author in (19). This information is of particular use to spacecraft design engineers who assess long term attitude performance of satellites.

2.4 Advantages of Gravity-Gradient Stabilization

There are several advantages to utilizing the naturally occurring gravitational torque in the design of spacecraft. A gravity-gradient stabilized spacecraft will maintain a stable orientation relative to the earth, without decaying or drifting due to other environmental torques. This assumes a stable environment (45:19). Gravity-gradient stabilization is one of several passive methods of stabilization. Passive methods require no spacecraft power consumption or ground-directed commands (45:19). With a position-controlled satellite, mission requirements may be met with a minimum of on-orbit satellites and the least

extensive and expensive system of ground stations (10). Another advantage of passive attitude control is the potential for very long satellite lifetimes. The operational life is not limited by onboard consummables or wear and tear on moving parts (6:297). Gravity-gradient stabilization is useful when long orbit lifetimes are needed and the attitude stability requirements are relatively broad (6:300). The operational utility of these satellites is explored further in Section 2.8.

2.5 Disadvantages of Gravity-Gradient Stabilization

While gravity-gradient stabilization does have its advantages, the method is not without some detrimental characteristics. The attitude of such a satellite is limited to only one or two possible orientations - the minimum inertia axis pointing toward or away from the center of the gravity field. This method is only effective near a massive central body, limiting its utility and preventing its application to certain planetary probes. Only specific satellite configurations permit the use of this stabilization method, since it requires the use of long booms or an elongated mass distribution. A gravity-gradient satellite is also subject to wobble or libration (45:19). Libration amplitudes of 10-20° are not uncommon (6:300). Furthermore, attitude control is limited to about 1°. Thermal gradients may easily develop across the length of the satellite or its deployable booms, contributing to both the libration and a decrease in attitude control (45:19). This problem is most likely related to the "unpredictable low frequency instability associated with solar radiation" addressed in (5). In one author's opinion, gravity-gradient stabilization is too imprecise and inflexible for most applications due to its poor overall accuracy and somewhat inflexible response to changing environmental conditions (6:300).

2.6 Equilibrium Orientations

It is at this point that the literature review becomes specifically pertinent to this particular study. Given the existence of relative equilibrium orientations, one would naturally speculate exactly how many equilibrium attitudes are produced by gravitational effects. Although no articles professing the existence of less than 24 equilibrium attitudes were located, several papers declared the existence of 24 or more equilibrium attitudes. The

reports described in this section all discuss whether or not gravitational effects produce *exactly* 24 or *at least* 24 equilibrium attitudes. This report and (42) appear to resume the debate.

According to (17), Lagrange was apparently the first to deduce from the relevant equations of motion the existence of 24 equilibrium attitudes. In these attitudes the body principal axes are aligned with the orbiting reference frame. He also investigated satellite librational motions and formulated stability conditions corresponding to the linearized dynamical equations. A similar result is obtained in (19) where the author claims that "a rigid body without an axis of symmetry, in a circular orbit, possesses 24 equilibria . . . which may be classified into six dynamically distinct groups each containing four elements."

The author of (17) continues by stating, "Most investigators appear to take for granted the uniqueness of the 24 classical equilibrium orientations. A contrary result, however, is claimed by a more recent paper . . . (22) . . . specifically, the existence of an infinite number of attitudes in which an arbitrary satellite can remain fixed in the orbiting frame." The work in (22) was refuted in (14) and again in (17) by the same author. Another paper, (33), considers a similar satellite and claims that "for a solid body with unequal moments of inertia moving in a circular orbit, there are *no equilibrium positions other than* those corresponding to the coincidence of the three principal central axes of inertia of the body with the axes of the orbital coordinate system." His solutions correspond to different cases for coincidence of the principal inertia axes of the body with the orbital coordinate system axes. The author then states that "this result demonstrates that the findings of Michelson [(22)] are not correct."

In their second attempt at describing the uniqueness of 24 equilibrium orientations, the authors of (14) and (17) derive equations for the attitude motion of a rigid body satellite in a circular orbit about a spherically symmetric earth. Additionally, the authors investigate the existence of equilibrium orientations in which the body maintains a fixed orientation with respect to an orbiting frame of reference, orientations corresponding to gravity-gradient stabilization positions (21). Intending to satisfy even the most cynical non-believers they reported on a mathematical development of the problem which reduces

to two eigenvalue problems with exactly 24 solutions. Clearly, not all were convinced, as can be seen in (40), (41), and (42).

As is described in this paper, the authors of (40), (41), and (42) examined the equations of motion pertaining to a rigid body of finite extent moving in a central gravitational field. These studies were intended to investigate the approximations inherent in models of a moving point mass. The authors questioned the common practice of retaining only the lowest-order, nonvanishing term of the gravitational potential. While non-great circle motions were shown to be impossible in the point mass model, relative equilibria were obtained through careful consideration of the exact gravitational potential acting on a finite body. The results of these papers decidedly conflict with those of (14), (33), and (17) and apparently may lend credence to the work in (22).

2.7 *Unique Ideas*

While a coauthor of (17) did adhere to the notion of *only* 24 equilibrium attitudes, he also recognized the possibility of what is referred to in (42) as "non-great circle orbits." He admits that the true orbit plane may be displaced from the nominal orbit plane such that the true orbit plane does not contain the gravitating center (32). He elaborates:

A point mass in an inverse square gravitational field can move in a circular orbit whose plane contains the gravitating center. In fact, the gravitating center must lie in the plane of the orbit, whatever conic the latter may be, because there is no force mechanism to generate or sustain any out-of-plane motion. On the other hand, a real material body is not a point mass and the gravitational force on such a distributed body depends on the orientation of the body about its center of mass. It is quite possible for the orbiting body to experience a force which is not collinear with the line from the attracting center to the center of mass of the body. (32)

As in (42), this author indirectly examined the effects of approximations of the gravitational potential and the different results obtained using finite body rather than point mass models.

Finally, one other work may have served as a precursor to the formulation of more exact equations of motion for a rigid body in a gravitational field. In (21), the effect of higher-order inertia integrals is investigated:

Under the assumption that the body dimensions are small relative to the radial distance from the center of force, terms in the third- and higher-order inertial integrals are ignored. However for a body with all three moments of inertia equal second-order terms in the gravitational torques are zero ... An analysis including the higher order inertia integrals shows that the attitude of an earth-pointing satellite with three equal moments of inertia may be rendered stable by the differential-gravity effects, provided the satellite is not spherically symmetric and no torques from other sources exist. (21)

Using the Liapounov direct method an expression for the gravitational potential was derived which included inertia integral terms through the fourth-order. His analysis showed that approximating the gravitational potential with only second-order inertia integrals is not always adequate. This would be particularly true when the three moments of inertia are equal or nearly equal (21).

2.8 Operations

Utilization of gravity-gradient stabilization has been documented in numerous articles and demonstrated in many fully-functioning satellites as well. This section describes a few examples.

In June 1963 the first orbiting vehicle to successfully achieve passive gravity-gradient attitude stabilization was launched. The space vehicle, designated 1963-22A or TRANSIT, was followed by 1963-38B, 1963-49B, and 1964-26A (23). These five spacecraft, designed by the Applied Physics Laboratory at The Johns Hopkins University, were instrumental in establishing the effectiveness of gravity-gradient stabilization. Although one began tumbling and stabilized upside down, improvements were made and lessons were learned. Stabilization problems were corrected on subsequent missions with the use of magnets, while thermal bending of the 100-foot booms was minimized by the use of an alternative material which was less absorptive. Using the silver-plated booms, the 12° amplitude of the high-frequency, dynamic boom bending was decreased to less than 0.25° (23).

The subject of booms arises frequently in the literature. In (5), it is postulated that the clever use of tip-weighted extendable booms on a spacecraft could provide three-axis passive stabilization, and thus a potentially desirable earth-pointing equilibrium attitude. Gravity-gradient stabilization achieved with dumbbell or boom configurations is also dis-

cussed in (31:83). The gravity-gradient loading on the long booms, exhibited during the boom-bending observed on mission 1963-22A, are mentioned also in (31:59). The torques on the booms cause the spacecraft to assume a radial attitude. In (6:299), the author explains that a typical method of obtaining the desired inertia properties for a spacecraft is to deploy a "motor-driven boom with a relatively heavy end mass." This can be accomplished by unrolling a reel of "prestressed metallic tape — like a carpenter's measuring tape" that forms a cylinder with significant lateral stiffness but minimal torsional rigidity (6:299). This particular type of boom is discussed in detail in (30). Since satellites equipped with long rigid booms cannot be deployed from the fairing of a rocket nose cone, the appendages must be extendable and retractable (31:83). One solution to this problem is the STEM - a storable tubular extendable member (30). A STEM is a strip of flat, thin material which forms a very strong tubular shape when extended. Coiled on a drum when stored, the STEM can provide a significant restoring torque as a gravity-gradient stabilizer (30).

Gravity-gradient stabilized satellites are useful for situations in which a particular instrument is designed to point in the zenith or nadir direction. This typically involves a specific inertia configuration in which the vehicle possesses an axis where $I_z \ll I_x, I_y$ (6:299). For example, the TRANSIT radio navigation satellite system's main requirement was a nadir-pointed antenna. These satellites exhibited 15-year lifetimes (6:297), (23). Although the Naval Research Laboratory (NRL) originally designed satellites to achieve pointing accuracy of $\pm 10^\circ$ (1), more recent techniques have permitted accuracies on the order of $1-3^\circ$ (6:309). GEOSAT, a US Navy radar altimetry satellite launched in 1984, achieved vertical stability to within 1° using an extremely stiff boom with an eddy current damper as its top mass (6:300). The use of gravity-gradient stabilization on lenticular communications satellites is presented in (11).

Even if a satellite is not designed to employ the stabilizing effects of gravity-gradient torques, its effect on operations must still be considered. For some applications, gravity-gradient effects may not be of significance. However, certain industrial manufacturing and materials-processing operations are best conducted in low gravity conditions. These

activities would need to take place near the center of mass or at a higher altitude where gravitational effects are diminished (6:64-65).

To summarize, volumes of material have been written on the subject of gravity-gradient stabilization and relative equilibria of rigid bodies in a central gravitational field. This chapter has provided a small sampling of some of the available, and possibly more interesting, results achieved in the last three decades. Three particularly useful sources are (13), (28), and (24). For further review, the reader is directed to the bibliographies found in the above references.

III. System Dynamics

3.1 Introduction

First, a development of the familiar gravity-gradient concept will be given, making special note of the approximations made in obtaining a result. Next an explanation of how this investigation differs from the typical gravity-gradient development will follow. Finally, the specific dynamical equations of interest to this study will be summarized.

3.2 Gravity-Gradient Development

Consider a rigid body, B , orbiting a large mass, B_0 , as shown in Figure 5. The gravitational attraction force experienced by each particle of the orbiting rigid body is

$$d\vec{F} = -\frac{GM}{|\vec{R} + \vec{r}|^2} \frac{\vec{R} + \vec{r}}{|\vec{R} + \vec{r}|} dm \quad (1)$$

where $(\vec{R} + \vec{r})/|\vec{R} + \vec{r}|$ is the unit vector in the direction from the center of the large body to the arbitrary mass particle, G is the universal gravitational constant, M is the mass of the large attracting body, \vec{R} is the vector from the center of mass of the attracting body to the center of mass of the orbiting body, and \vec{r} is the vector from the center of mass of the orbiting body to each individual mass particle (8). Simplifying and integrating over the entire body to obtain the total gravitational force imparted onto the orbiting body we see that

$$\vec{F} = -GM \int_B \frac{\vec{R} + \vec{r}}{|\vec{R} + \vec{r}|^3} dm = m\ddot{\vec{R}} \quad (2)$$

where \int_B indicates the integral over the orbiting rigid body.

As is frequently done in astronomical calculations, algebraic manipulation followed by an approximation and subsequent Taylor series expansion simplify matters significantly. Algebraic manipulation of the denominator of the integrand in Equation 2 yields

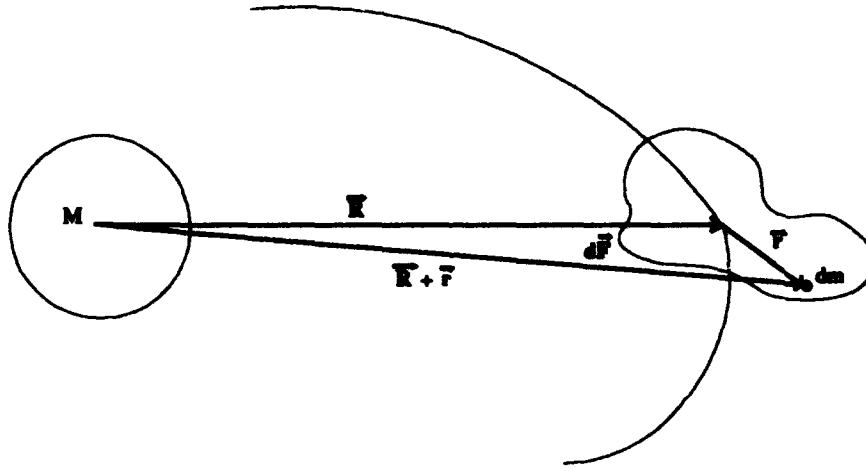


Figure 5. A rigid body orbiting a massive central body under the influence of a gravitational field.

$$\begin{aligned}
 \frac{1}{|\vec{R} + \vec{r}|^3} &= \frac{1}{[|\vec{R}|^2 + 2\vec{R} \cdot \vec{r} + |\vec{r}|^2]^{\frac{3}{2}}} \\
 &= \frac{1}{|\vec{R}|^3 \left[1 + 2\frac{\vec{R} \cdot \vec{r}}{|\vec{R}|^2} + \frac{|\vec{r}|^2}{|\vec{R}|^2} \right]^{\frac{3}{2}}}
 \end{aligned} \tag{3}$$

Now we assume $|\vec{r}| \ll |\vec{R}|$, neglect terms including $|\vec{r}|^2/|\vec{R}|^2$, and apply a Taylor series expansion, $(1+x)^{-n} = 1 - nx$, to obtain

$$\frac{1}{|\vec{R} + \vec{r}|^3} \approx |\vec{R}|^{-3} \left[1 - 3\frac{\vec{R} \cdot \vec{r}}{|\vec{R}|^2} \right] \tag{4}$$

Substituting this expression into Equation 2 we get

$$\vec{F} \approx -\frac{GM}{|\vec{R}|^3} \int_B (\vec{R} + \vec{r}) \left[1 - 3\frac{\vec{R} \cdot \vec{r}}{|\vec{R}|^2} \right] dm \tag{5}$$

and

$$\vec{F} \approx -\frac{GM}{|\vec{R}|^3} \int_B (\vec{R} + \vec{r}) dm + \frac{GM}{|\vec{R}|^3} \int_B \frac{(\vec{R} + \vec{r})(3\vec{R} \cdot \vec{r})}{|\vec{R}|^2} dm \quad (6)$$

As has been done for centuries, an approximation is then made by neglecting higher order terms and retaining only the first nonzero term. After acknowledging that the integral of $\vec{r} dm$ over the body vanishes we then obtain

$$\vec{F} \approx -\frac{GMm}{|\vec{R}|^3} \vec{R} \quad (7)$$

and finally

$$m\ddot{\vec{R}} + \frac{GMm}{|\vec{R}|^3} \vec{R} \approx \vec{0} \quad (8)$$

The same result may also be obtained if the orbiting body is spherically symmetrical, or originally defined as a point mass.

A similar development of the accompanying moment equation and an examination of the balance of angular momentum for a circular orbit yield the familiar gravity-gradient concept: by aligning two principal axes with the orbit normal and the radius vector to the central body, equilibrium is obtained. Thus there are 24 possible equilibrium configurations of a gravity-gradient body in a circular orbit — 3 axes to align with the radius vector times 2 directions per axis times 4 axes to align with the orbit normal (46), (17). Not all 24 of these are stable of course, as is shown in (46:148), (19), and (13:294-307). Similar developments of the gravity-gradient tensor can be found in (45:128), while an expression for total gravity gradient load as a function of mass, length, angular velocity and vertical displacement angle is located in (31). An expression for gravity-gradient torque is also given in (6:293). Development of the gravity-gradient geopotential and a discussion of harmonics are provided in (20:430-438).

The operational significance of this gravity-gradient finding has been described in numerous works such as (28), (10), (11), (23), and (6). Several satellites have incorporated this type of passive stabilization, namely, the Transit-5A, GGTS (Gravity Gradient Test Satellite), DODGE (Department of Defense Gravity Experiment), GEOS (Geodetic Earth

Orbiting Satellite), RAE-2 (Radio Astronomy Explorer), NRL 164, Salyut 6, and LDEF (Long Duration Exposure Facility) (45:787), (5), (13:327,334,336,339,341).

3.3 A Gravity-Gradient Alternative

The premise of this investigation is almost exclusively based on the results of (42). This section contains a brief overview of the dynamical equations of interest. The reader is referred to (40), (41), and (42) for a detailed account of the theoretical development of the relevant equations of equilibrium discussed here.

As an alternative formulation to Equation 8, consider again the motion of a rigid body B^* under the influence of a central inverse-square gravitational force due to a massive body B_o^* . Because the massive body is assumed to be stationary, a restricted two-body approach is applicable. An inertial reference frame is located at the origin O , the mass center of the stationary massive body. As shown in Figure 6, with C designated as the mass center of the rigid body in motion, \vec{r}^* denotes the vector from O to C in the inertial frame and \vec{Q}^* is the vector from C to an arbitrary point in the rigid body in the body frame. B is the transformation matrix from the body frame to the inertial frame. The mass particle associated with the arbitrary point will be denoted by $dm(\vec{Q}^*)$.

It is easily seen that the linear momentum and angular momentum of B about O , expressed in the inertial frame are

$$\vec{p}^* = \int_{B^*} \frac{d}{dt}(\vec{r}^* + B\vec{Q}^*)dm(\vec{Q}^*) = m\dot{\vec{r}}^* \quad (9)$$

and

$$\vec{\pi}^* = \int_{B^*} (\vec{r}^* + B\vec{Q}^*) \times \frac{d}{dt}(\vec{r}^* + B\vec{Q}^*)dm(\vec{Q}^*) \quad (10)$$

$$= \vec{r}^* \times m\dot{\vec{r}}^* + B\Gamma^*\vec{\Omega}^* \quad (11)$$

where

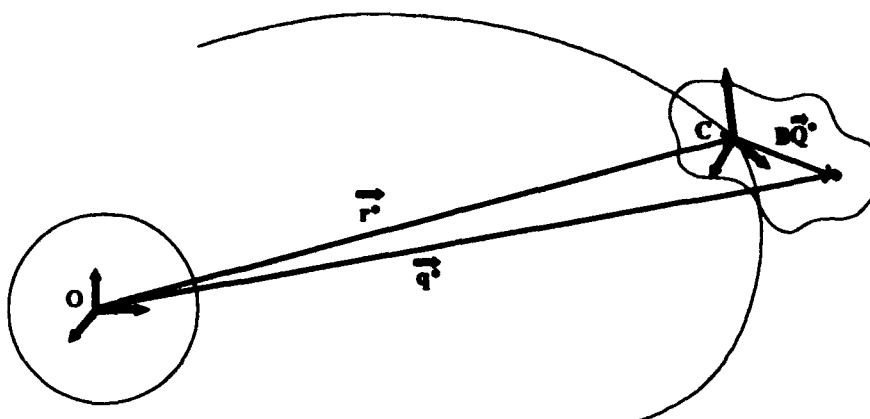


Figure 6. A rigid body in a central gravitational field.

- m = mass of the moving rigid body
 \vec{p}^* = linear momentum
 $\vec{\pi}^*$ = angular momentum
 $\vec{\Omega}^*$ = instantaneous angular velocity in the body frame
 I^* = the moment of inertia matrix of B^* in the body frame

and the dot indicates a derivative with respect to time while the superscript * denotes a quantity with dimension (for reasons which will soon be apparent). The moment of inertia matrix I^* is written as

$$I^* = \int_{B^*} \widehat{Q}^* \widehat{Q}^{*T} dm(\vec{Q}^*) \quad (12)$$

where \widehat{Q}^* indicates the skew-symmetric matrix

$$\begin{pmatrix} \widehat{Q}_1^* \\ \widehat{Q}_2^* \\ \widehat{Q}_3^* \end{pmatrix} = \begin{pmatrix} 0 & -Q_3^* & Q_2^* \\ Q_3^* & 0 & -Q_1^* \\ -Q_2^* & Q_1^* & 0 \end{pmatrix} \quad (13)$$

The primary body is assumed to be spherically symmetric and the resulting potential field produced by B^* is

$$V = - \int_{B^*} \frac{GM}{|\vec{r}^* + B\vec{Q}^*|} dm(\vec{Q}^*) \quad (14)$$

where M is the mass of B^* . Assuming that no external forces are acting on the two-body system, the resultant force on B^* , with $\vec{F} = \nabla V$, is

$$\vec{F} = - \int_{B^*} \frac{GM(\vec{r}^* + B\vec{Q}^*)}{|\vec{r}^* + B\vec{Q}^*|^3} dm(\vec{Q}^*) = \dot{\vec{p}}^* \quad (15)$$

This result arises since balance of linear momentum implies that the sum of forces is equal to the time rate of change of linear momentum. Note that the final force expression in Equation 7 is different from the one just developed in Equation 15. Multiplying this force term by a moment arm to obtain a torque, assuming there are no external couples acting on B^* , yields

$$\vec{\tau} = - \int_{B^*} (\vec{r}^* + B\vec{Q}^*) \times \frac{GM(\vec{r}^* + B\vec{Q}^*)}{|\vec{r}^* + B\vec{Q}^*|^3} dm(\vec{Q}^*) = \vec{0} \quad (16)$$

which then implies, through balance of angular momentum,

$$\dot{\vec{\pi}}^* = \vec{0} \quad (17)$$

Now the substitution $\vec{\Pi}^* = I^* \vec{\Omega}^*$ is made, with $\vec{\Pi}^*$ denoting the instantaneous body angular momentum of B^* . Furthermore, the equations are now expressed in the body frame through the following vector body variables:

$$\lambda^* = B^T \vec{r}^* \quad \mu^* = B^T \vec{p}^* \quad (18)$$

The equations of equilibrium may now be written as

$$\dot{\Pi} = \Pi^* \times I^{*-1} \Pi^* + \int_{B^*} \frac{GM(\lambda^* \times Q^*)}{|\lambda^* + Q^*|^3} dm(Q^*) \quad (19)$$

$$\dot{\lambda}^* = \lambda^* \times I^{*-1} \Pi^* + \frac{\mu^*}{m} \quad (20)$$

$$\dot{\mu}^* = \mu^* \times I^{*-1} \Pi^* - \int_{B^*} \frac{GM(\lambda^* + Q^*)}{|\lambda^* + Q^*|^3} dm(Q^*) \quad (21)$$

$$\dot{B} = B \widehat{I^{*-1} \Pi^*} \quad (22)$$

The system is then nondimensionalized with mass, length, and time scales

$$m \quad l = \left(\frac{\text{tr}(I^*)}{m} \right)^{\frac{1}{2}} \quad T = \left(\frac{l^3}{GM} \right)^{\frac{1}{2}} \quad (23)$$

and nondimensional variables

$$\lambda \equiv \frac{\lambda^*}{l} \quad \mu \equiv \frac{\mu^*}{mlT^{-1}} \quad \Pi \equiv \frac{\Pi^*}{ml^2T^{-1}} \quad t \equiv \frac{t^*}{T} \quad (24)$$

By converting the rigid body B^* into a nondimensional body B , the following definitions arise from the dimensional mass differential dm ,

$$Q = \frac{Q^*}{l} \quad (25)$$

$$d\nu(Q) = \frac{1}{m} dm(Q^*) \quad (26)$$

$$\int_B d\nu(Q) = \int_{B^*} \frac{1}{m} dm(Q^*) = 1 \quad (27)$$

where the nondimensional moment of inertia of B is defined as

$$I = \frac{I^*}{\text{tr}(I^*)} \quad (28)$$

and $\text{tr}(I) = 1$. The dynamic equations can now be expressed with the nondimensional variables as

$$\Pi' = \Pi \times I^{-1}\Pi + \int_B \frac{\lambda \times Q}{|\lambda + Q|^3} d\nu(Q) \quad (29)$$

$$\lambda' = \lambda \times I^{-1}\Pi + \mu \quad (30)$$

$$\mu' = \mu \times I^{-1}\Pi - \int_B \frac{\lambda + Q}{|\lambda + Q|^3} d\nu(Q) \quad (31)$$

$$B' = B \widehat{I^{-1}} \Pi \quad (32)$$

with the prime denoting a derivative with respect to the nondimensional time t . Since Equations 29-31 do not include the attitude B , they are decoupled from Equation 32. Also, since the states of interest in this investigation are those of relative equilibria, where the rigid body B^* spins steadily about O while the center of mass C remains in a circular orbit, Equations 29-31 may be set equal to zero. Therefore, the reduced equations of equilibrium are

$$\Pi \times I^{-1}\Pi + \int_B \frac{(\lambda \times Q)}{|\lambda + Q|^3} d\nu(Q) = \vec{0} \quad (33)$$

$$\lambda \times I^{-1}\Pi + \mu = \vec{0} \quad (34)$$

$$\mu \times I^{-1}\Pi - \int_B \frac{\lambda + Q}{|\lambda + Q|^3} d\nu(Q) = \vec{0} \quad (35)$$

Through a series of manipulations involving Hamiltonians, Casimir functions, and variational methods, the dynamical equations are then reduced to

$$(I + \hat{\lambda}^T \hat{\lambda}) \Omega = \beta \Omega \quad (36)$$

$$\hat{\Omega}^T \hat{\Omega} \lambda = \int_B \frac{\lambda + Q}{|\lambda + Q|^3} d\nu(Q) \quad (37)$$

$$\frac{1}{2} |\Omega|^2 = c \quad (38)$$

where β is a lagrange multiplier with a value of $-|\lambda|^2$ and c is a constant from variational principles (42).

These are the generalized equations of equilibrium considered in this report. Of particular significance is the fact that the gravitational potential term in these equations was not approximated and remains exact. The use of the *exact* model is the key difference between this approach and the gravity-gradient approach developed earlier.

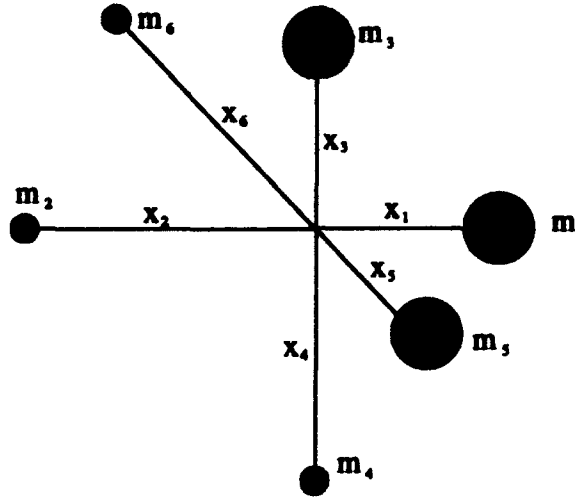


Figure 7. A rigid body satellite modelled as a molecule.

As in (42), the model used to discover and demonstrate these non-great circle orbits consists of six mass particles connected by three rigid rods whose mass is considered negligible. Two of the point masses lie at opposite ends of each of the three principal axes. The three rods form an orthonormal body frame and coincide with the three principal axes. The molecule model is shown in Figure 7. Transforming the integral in equation 37 to a summation yields the following model-specific equations:

$$|\Omega|^2 \lambda - (\Omega \cdot \lambda) \Omega - A \sum_{i=1}^6 \frac{m_i (\lambda + Q_i)}{|\lambda + Q_i|^3} = 0 \quad (39)$$

$$I \Omega + |\lambda|^2 \Omega - (\Omega \cdot \lambda) \lambda - \beta \Omega = 0 \quad (40)$$

$$\frac{1}{2} |\Omega|^2 - c = 0 \quad (41)$$

where A is a parameter introduced to minimize numerical ill-conditioning. The value of A was chosen to be $0.04|\lambda|^5$. A complete description of the methodology used to arrive at this value is given in (42). The preceding equations serve as the departure point from which the remaining analysis proceeds.

IV. Methodology

4.1 Model Description

As seen in Figure 7, the model used in this investigation consists of 6 point masses attached to the ends of 3 mutually perpendicular massless rods. The exact configuration of masses and rod lengths was chosen to maximize the effect of higher order terms, accomplished by specifying moments of inertia close to each other and insuring the model is highly asymmetric. As described in (42), the masses and moments of inertia were chosen as follows:

$$\begin{aligned} m_1 &= 0.330066 & m_2 &= 0.00330033 \\ m_3 &= 0.330033 & m_4 &= 0.00330033 \\ m_5 &= 0.33 & m_6 &= 0.00330034 \\ I_1 &= 0.3332 & I_2 &= 0.3335 & I_3 &= 0.3333 \end{aligned} \quad (42)$$

These choices satisfy the constraints imposed by the nondimensionalization:

$$\sum_{i=1}^6 m_i = 1 \quad \sum_{i=1}^6 m_i x_i^2 = 0.5 \quad (43)$$

where the second constraint arises from $\text{tr}(\mathbf{I}) = 1$.

In order to analyze numerically the equations of motion on a computer, equations 39-41 were written in a form which could be readily converted to Fortran code. Similarly, the Jacobian, $f'(\lambda, \Omega, \beta)$, of Equations 39-41 was required to perform the continuation technique utilized in obtaining relative equilibria. The Fortran representation of both the function f and the Jacobian f' are provided in Appendix A.

The dynamic equations were coded and validated in double precision (REAL*8) on a Sun SparcStation. Validation included a comparison of the values of $f(\lambda, \Omega, \beta)$ and $f'(\lambda, \Omega, \beta)$ obtained using the code in Appendix A and those obtained by using the program developed for (42). The function code was then incorporated into an AUTO subroutine and tested for proper integration within the software.

4.2 Continuation Method

Relative equilibria were found by solving the system $f(\lambda, \Omega, \beta) = 0$ using a Newton-Raphson method. The method will be introduced here first in scalar form. As described in (26), (29), (2:153), and (7), the Newton-Raphson method may be derived from a Taylor series expansion, which can be represented as

$$f(x_{i+1}) = f(x_i) + f'(x_i)(x_{i+1} - x_i) + \frac{f''(\zeta)}{2}(x_{i+1} - x_i)^2 \quad (44)$$

where ζ is somewhere in the interval between x_i and x_{i+1} . An approximation may be made by truncating Equation 44 after the first derivative term:

$$f(x_{i+1}) \simeq f(x_i) + f'(x_i)(x_{i+1} - x_i) \quad (45)$$

Since we are trying to solve for $f(x) = 0$, $f(x_{i+1})$ would be equal to zero at the intersection with the x axis. This observation yields

$$0 \simeq f(x_i) + f'(x_i)(x_{i+1} - x_i) \quad (46)$$

which can then be solved for x_{i+1} as

$$x_{i+1} = x_i - \frac{f(x_i)}{f'(x_i)} \quad (47)$$

The exact method used in this study follows a similar development, although the vector form is slightly different than the scalar form described above. Beginning with an initial known solution $f(u_o, \eta_o) = 0$, where u indicates the states and η is a parameter, a new solution $f(u, \eta)$ is desired. First, an Euler step is taken where $\eta = \eta_o + \Delta\eta$. We now seek

$$f(u_o + \Delta u, \eta_o + \Delta\eta) = 0 \quad (48)$$

Using a multi-variable form of the Taylor series expansion we see that

$$\begin{aligned}
0 &= f(u_o + \Delta u, \eta_o + \Delta \eta) \\
&= f(u_o, \eta_o) + f_u(u_o, \eta_o)\Delta u + f_\eta(u_o, \eta_o)\Delta \eta + \text{higher order terms}
\end{aligned} \tag{49}$$

where f_u is the matrix of partial derivatives of f with respect to u , also known as the Jacobian, J , and f_η is the matrix of partial derivatives of f with respect to η . Setting the initial solution equal to zero and solving for Δu yields

$$\Delta u = -J^{-1}(u_o, \eta_o)f_\eta(u_o, \eta_o)\Delta \eta \tag{50}$$

which in turn gives a first approximation for a new value of u

$$u_n = u_o - J^{-1}(u_o, \eta_o)f_\eta(u_o, \eta_o)\Delta \eta \tag{51}$$

Now, a Newton step is taken to improve upon the most recent value of u . Keeping the same value of η , we now desire $f(u_n + \Delta u, \eta) = 0$. As before,

$$f(u_n, \eta) + J(u_n, \eta)\Delta u + \text{higher order terms} = 0 \tag{52}$$

and

$$\Delta u = -J^{-1}(u_n, \eta)f(u_n, \eta) \tag{53}$$

which produces a better estimate of u in the form of

$$u_{n+1} = u_n - J^{-1}(u_n, \eta)f(u_n, \eta) \tag{54}$$

Proceeding in this manner allows one to vary the parameter, η , and obtain successive solutions to the original function f . Using the notation of the particular dynamical system examined in this study, branches of equilibrium points could be determined by starting with an initial solution for $f(\lambda, \Omega, \beta, c)$ and incrementing the parameter, c . The process of estimating and improving successive values of a state vector may be referred to as pre-conditioning. The path following method described here and other methods of pre-conditioning are explained in further detail in (44).

4.3 Utilizing AUTO86

A continuation software package called AUTO86 (4), written by Eusebius Doedel, was used to trace solution branches in this study. AUTO contains algorithms capable of solving a system of algebraic equations $f(u, \eta) = 0$, where u is a set of states and η denotes one or more variable parameters. The software is also capable of detecting algebraic bifurcation points and limit or turning points along a solution branch. The reader is referred to (35) for an explanation of bifurcation and limit points.

An initial solution for a particular value of the parameter, η , is used as input for AUTO to begin its continuation routine. From the starting point, the parameter is varied in a stepwise fashion and a new solution is traced using a pseudo-arclength continuation technique (4). User-supplied subroutines are also required to calculate the function $f(u, \eta)$, the Jacobian $f'(u, \eta)$, and to initialize certain program constants.

From the equations

$$f(u_j, \eta_j) = 0 \quad (55)$$

$$\theta_u^2(u_j - u_{j-1})^T \dot{u}_{j-1} + \theta_\eta^2(\eta_j - \eta_{j-1})^T \dot{\eta}_{j-1} - \Delta s = 0 \quad (56)$$

where Δs is the stepsize along the branch, the next solution is computed. θ_u and θ_η are preassigned constants used to indicate scaling differences between u and η . The stepsize may be fixed or adaptive. For an adaptive stepsize in which the Newton iteration routine fails to converge, the stepsize is halved. For an adaptive stepsize in which the Newton iteration routine converges rapidly, the stepsize is increased. However, the stepsize is not permitted to proceed beyond a user-selected minimum and maximum. Convergence criteria are also selected by the user. Convergence is reached if the Newton increments satisfy

$$\frac{|\delta\eta|}{1 + |\delta\eta|} < \epsilon_\eta \quad \text{and} \quad \frac{\|\delta u\|_\infty}{1 + \|u\|_\infty} < \epsilon_u \quad (57)$$

where ϵ_η and ϵ_u are selected by the user (4).

4.4 Accuracy Testing

Some of the AUTO subroutines were modified and others were added to explicitly establish the accuracy of a computed equilibrium solution. As described in (42), (25), and (26), the Kantorovich theorem may be used to measure the error for a solution and serve as a criterion for convergence. Consequently, additional calculations were made to determine the necessary coefficients for the Kantorovich theorem. The following constraints were used in accepting an AUTO-derived equilibrium point:

$$\alpha\sigma\gamma \leq \frac{1}{2} \quad \text{and} \quad \gamma < \epsilon \quad (58)$$

where

$$\begin{aligned} \alpha &= 2n|\lambda| \\ n &= \text{number of equations} = 7 \\ \sigma &= \frac{n}{\rho_{min}} \\ \rho_{min} &= \text{minimum eigenvalue of } f'(\lambda, \Omega, \beta) \\ \gamma &= \|\delta u\|_{\infty} = \max(\delta u_i, i = 1, 2, \dots, 7) \end{aligned}$$

and ϵ is a user-specified error bound. If these constraints are satisfied, the order of convergence is guaranteed to be at least quadratic (25).

Insufficient accuracy was obtained using the Sun workstation, therefore the code was transferred to the Ohio Supercomputer Cray where double precision accuracy to 29 digits was possible (29). Even after this was accomplished, accuracy still did not appear to correlate with the results achieved in (42). Thus, a gaussian elimination subroutine in AUTO was replaced with a singular value decomposition (SVD) subroutine obtained in (27). The SVD routine was thought to be a more robust algorithm well-suited for such an ill-conditioned problem.

4.5 Procedure

Significant importance was given to reproducing Table 2 of (42). Once those results could be duplicated and verified, continued analysis of the anomalous behavior at certain

points of the equilibrium branch could begin. In the interest of clarity, Table 2 of (42) is shown here as Table 1 where the solution numbers have been added to assist in identification. The table is segmented according to the three presumed equilibrium branches represented.

Table 1. Relative Equilibria Illustrating Large Orientation Drifts (42)

Solution	$ \lambda $	$\theta(\lambda)$	$\phi(\lambda)$	$ \Omega $	$\theta(\Omega)$	$\phi(\Omega)$
1	500	46.8611	-17.4627	100	-54.7456	-32.6009
2	760	47.8276	-17.8208	152	-54.7761	-34.1683
3	1000	48.7091	-18.1277	200	-54.8384	-35.5845
4	3000	55.3232	-17.2751	600	-20.2429	38.7129
5	6000	65.6627	-19.5986	1200	-15.6572	22.9702
6	8000	71.0045	-22.9513	1600	-11.4520	17.2236
7	9000	73.0742	-25.3278	1800	-9.5049	15.2639
8	12000	78.0382	22.8848	2400	-7.5808	-10.2578
9	15000	81.2009	18.9175	3000	-6.4284	-6.8820
10	20000	84.1137	13.7814	4000	-4.9693	-3.7331
11	30000	86.5362	8.1721	6000	-3.2604	-1.4159
12	40000	87.5514	5.6183	8000	-2.3792	-0.7051

The numerical analysis began by converting the data in Table 1 to cartesian coordinates and using a specific solution, or solution number, as the initial starting point for AUTO. In particular, efforts were made to trace equilibrium branches which encompassed data from Solutions 1 to 4, Solutions 4 to 1, Solutions 3 to 8, Solutions 8 to 3, Solutions 8 to 12, and Solutions 12 to 8. Distinction is made between solutions with increasing versus decreasing λ since this method was intended to locate the bifurcation points implied by discontinuities found between Solutions 3 and 4 and Solutions 7 and 8.

Certain variables in the AUTO software were extremely sensitive and required adjustment for each initial solution in order to produce an equilibrium branch. Consequently, several hundred runs using a trial and error process were required to obtain results resembling valid data.

Those equilibrium states that were obtained were converted to spherical coordinates: $\lambda = (r \cos \phi \cos \theta, r \cos \phi \sin \theta, r \sin \phi)$ for comparison to the results found in (42), and to

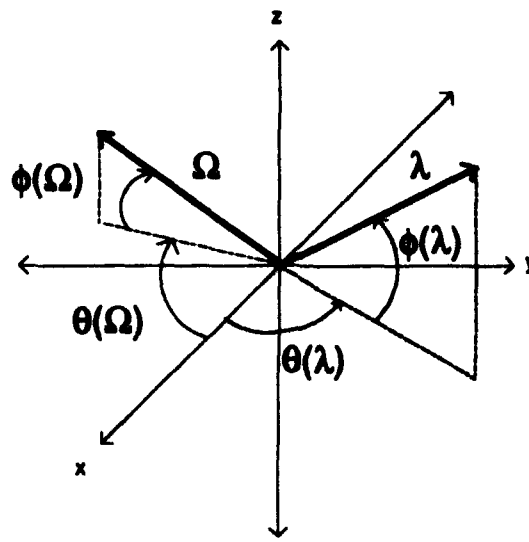


Figure 8. Spherical Coordinate System.

aid in graphical representation. The spherical coordinate system used is provided in Figure 8.

V. Results

5.1 Introduction

Efforts to duplicate Table 1 met with partial success. In general, it appears as though the results of (42) can be validated, but not with the ease expected from using the AUTO software package. The intent was to perform a complete turning point and bifurcation analysis using AUTO, particularly in the regions where Table 1 indicated discontinuities. A few bifurcation points were detected but certain convergence tests were not met and the data was deemed invalid. The data obtained thus far indicates that the solutions in Table 1 are in fact equilibrium solutions, but the continuous branches suggested by (42) could only be reproduced by using the same program employed in (42). Preliminary results implied the existence of not three, but at least twelve branches corresponding to each solution of Table 1; however, this outcome was attributed to numerical instabilities present in the utilization of AUTO for this particular dynamical system. All results, including those considered defective, were obtained at significant computational expense, possibly due to these instabilities. Specific results are described in the following section.

5.2 Discussion of Results

As stated earlier, a primary objective of this study was the reproduction of selected results from (42), shown in Table 1. Figure 9 is a graphical representation of Table 1 with missing data supplied by interpolation and represented by dashed and dotted (---) lines. Figure 10 depicts the results obtained from several versions of code and numerous program runs. Throughout the figures in this section, data from Table 1 is also included for comparison purposes. Furthermore, of the six major equilibrium solution components, λ , $\theta(\lambda)$, $\phi(\lambda)$, Ω , $\theta(\Omega)$, and $\phi(\Omega)$, only two, $\phi(\Omega)$ and λ , were chosen to graphically represent these results since a plot of $\phi(\Omega)$ most clearly indicates the existence of three distinct equilibrium branches.

As can be inferred from Figure 10, only a partial mapping of the complete phase space was accomplished. However, AUTO was able to converge on the initial starting solutions obtained from Table 1, but quickly diverged from the expected solutions. Many equilibrium

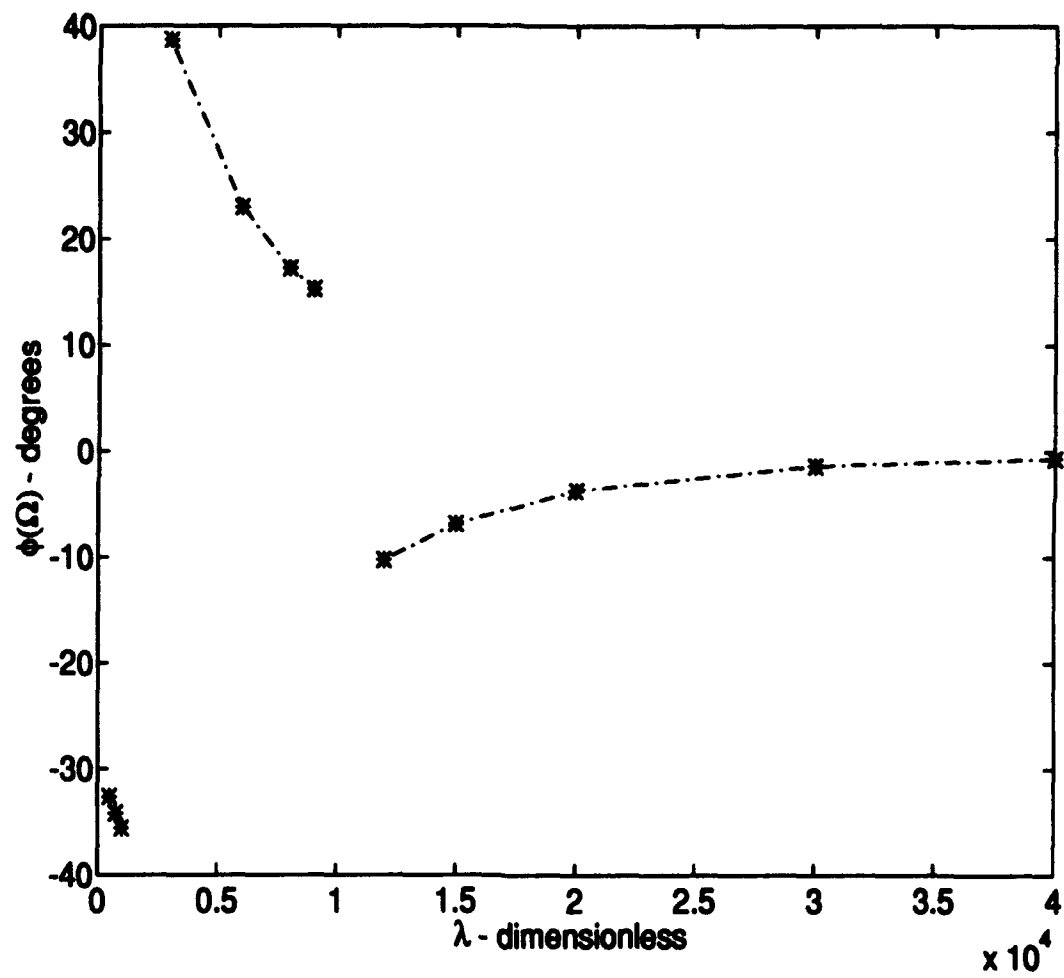


Figure 9. Interpolated Data from Table 1.

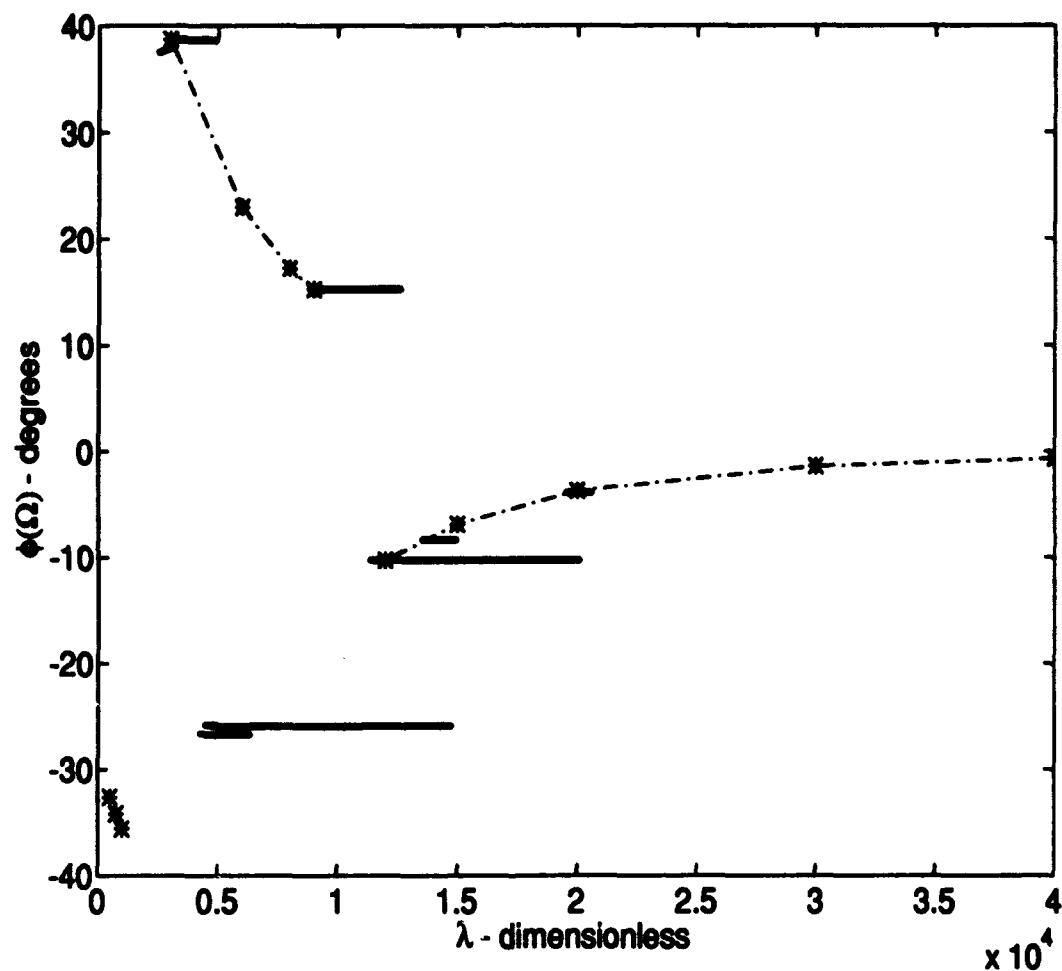


Figure 10. The results from AUTO are depicted as a thick line of connected dots while the interpolated results from Table 1 are displayed by asterisks and dash-dot lines. Additional AUTO results are found close to the Table 1 cluster located between -30 and -40 degrees, but are not visible using this scale.

solutions were found which cannot be seen in Figure 10 due to the chosen scale. These are explored in later figures. Additionally, an equilibrium branch not obtained in (42) appears to exist between $\phi(\Omega)$ values of -20° and -30° . The additional branch was obtained when NEWT failed to converge on a nearby solution. NEWT is the program originally used in (42) to iterate on an initial state using Equations 39-41 until convergence on a nearby solution occurs. An AUTO run starting from Solution 4 terminated prematurely. The final solution obtained from this run was used as an initial state in NEWT, which then converged on a very different solution. It is this state which was used as a starting solution for the results found between -20° and -30° . Section 5.5 elaborates.

The following presentation of results expands upon Figure 10 by dividing the region into five ranges corresponding to areas of interest in Table 1. Range 1 includes equilibria found with λ values between 500 and 1000, corresponding to Solutions 1 and 3. Similarly, the remaining ranges are allotted according to Table 2.

Table 2. Definition of ranges used in displaying results.

Range	Min λ value	Max λ value	Starting Solution	Ending Solution
1	500	1000	1	3
2	1000	3000	3	4
3	3000	9000	4	7
4	9000	12000	7	8
5	12000	40000	8	12

Figure 11 shows the equilibria obtained with Solutions 1, 2, and 3. Figure 12 shows an enlargement of the equilibria obtained with an initial starting solution from Solution 1. The solutions near -32.65° were obtained after AUTO's restart option did not function. The last available solution was then iterated upon in NEWT and the new starting solution it produced was used for an additional AUTO run. It should be noted that although the AUTO results appear to produce a constant $\phi(\Omega)$, the variable does decrease as expected, although not at the rate implied by interpolated Table 1 results. AUTO output with Solution 3 as the starting solution is shown in Figure 13.

Results from the end of Range 2 are shown in Figure 14. The starting solution for this data was Solution 4. In an effort to explore the discontinuity present in the data,

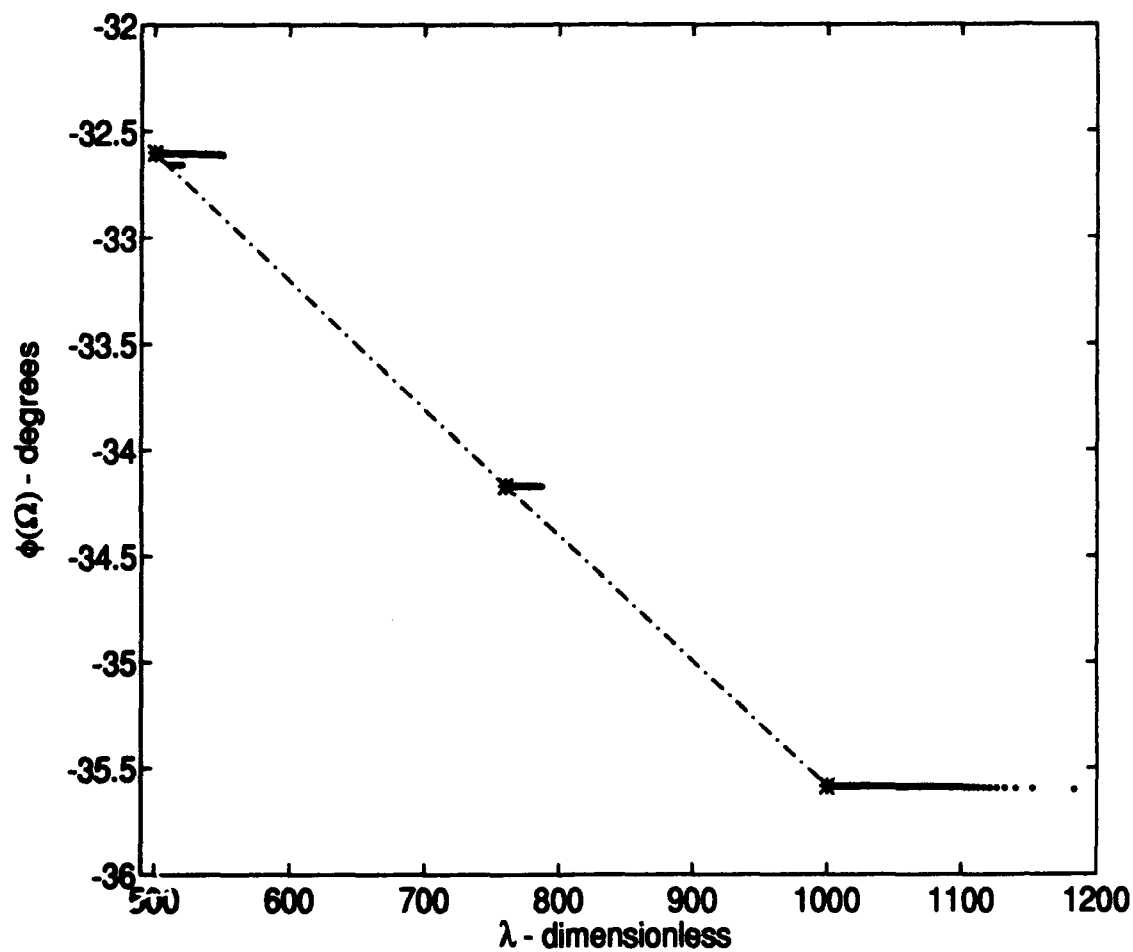


Figure 11. AUTO results in Range 1 are depicted by dots while interpolated data from Table 1 is shown by a dash-dot line.

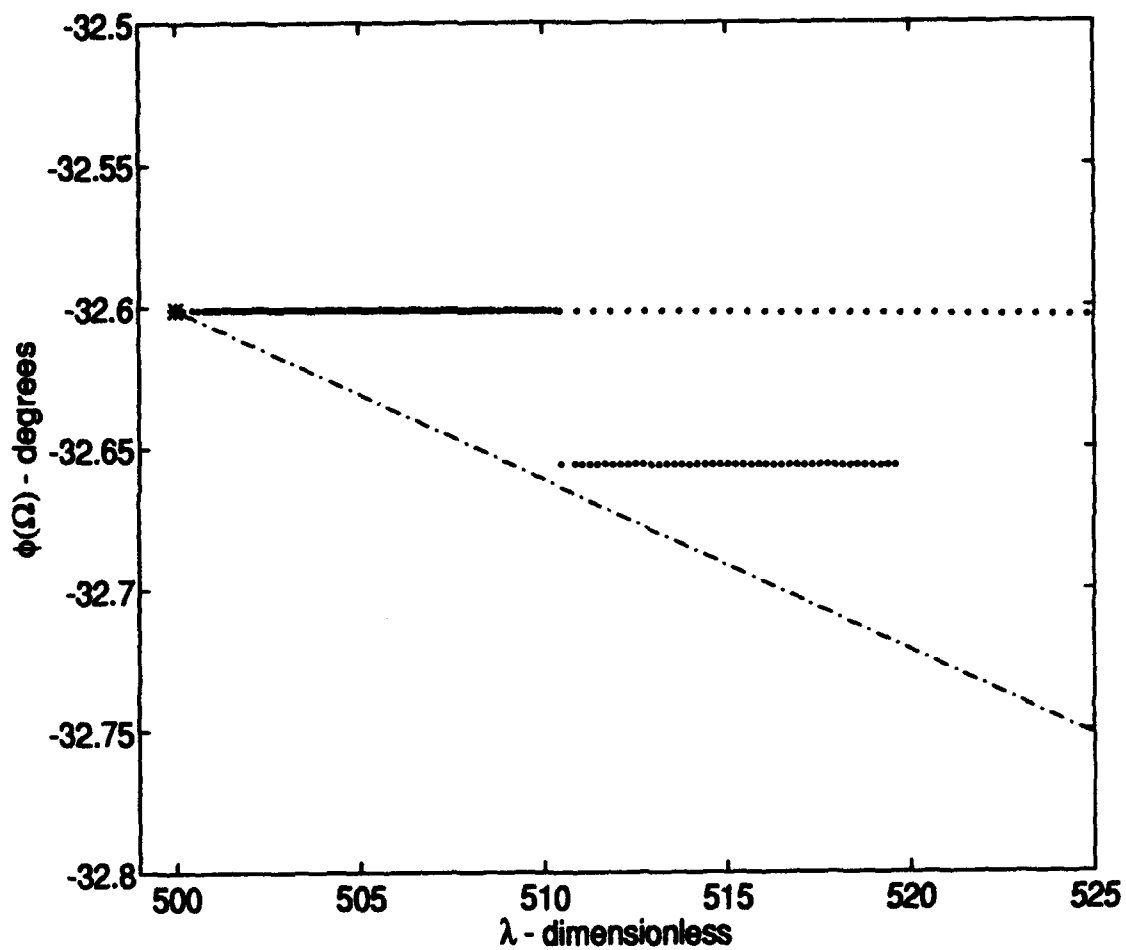


Figure 12. Enlarged AUTO results in Range 1 are depicted by dots while interpolated data from Table 1 is shown by a dash-dot line.

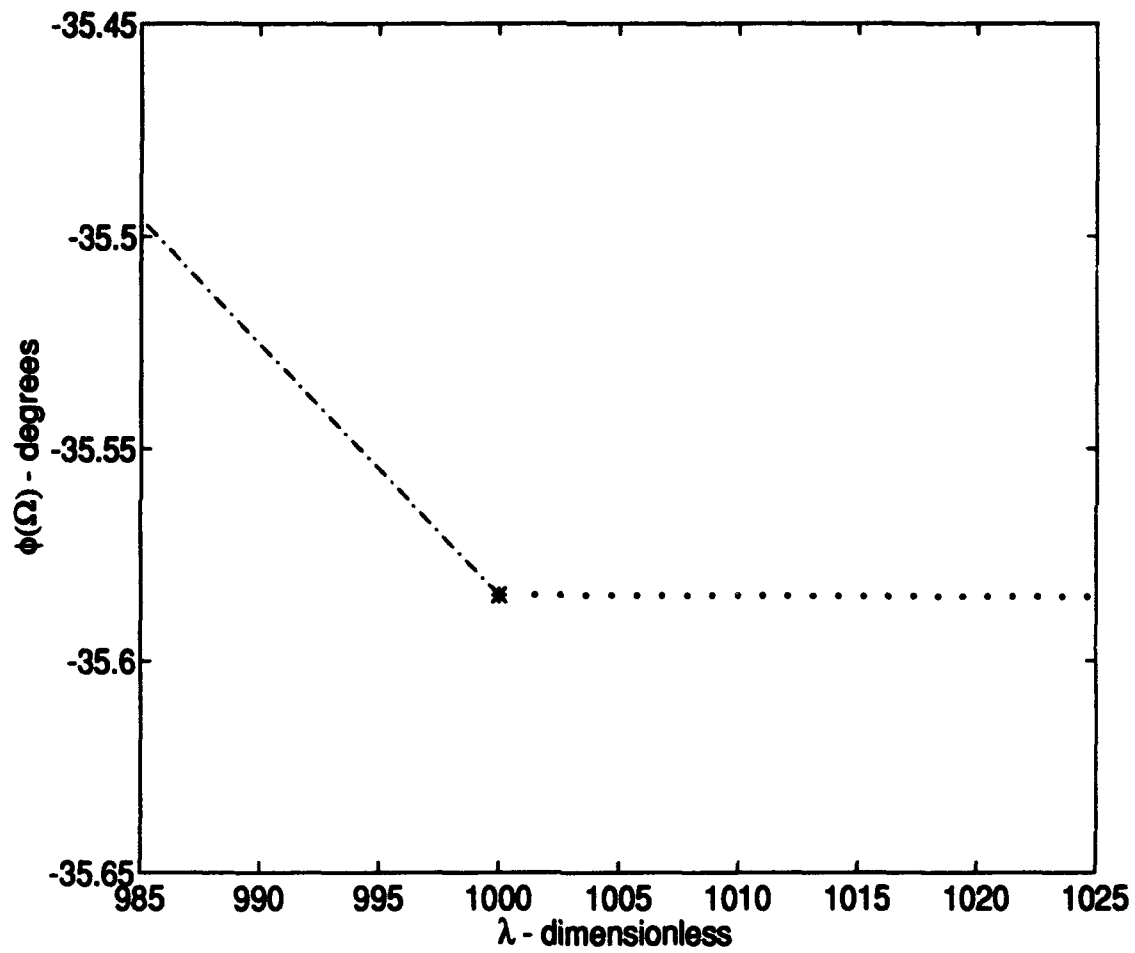


Figure 13. AUTO results in Range 2 are depicted by dots while interpolated data from Table 1 is shown by a dash-dot line.

each solution obtained from this run was iterated upon in NEWT, thereby arriving at a NEWT-refined solution from each AUTO solution. The results of the refinement process are shown in Figure 15. The NEWT data has been partially filtered to eliminate spurious results attributed to the lack of significant digits available on a Sun workstation. As would be expected, the solutions are nearly identical. However, it is interesting that the slope of the NEWT data is of higher magnitude than the AUTO data.

Figure 16 depicts the AUTO solutions shown in Figure 14 and those obtained from a NEWT starting solution. As mentioned above, after an unsuccessful restart attempt the last available AUTO solution, with Solution 4 as the initial state, was used in NEWT to arrive at a very different solution. Executing AUTO with this starting solution yielded the results shown in Figure 16. Figure 17 is an enlarged view of the potential new branch(es). Although Figure 17 depicts four potential branches, the discontinuities are assumed to be a result of numerical instabilities identical to those which produced the results in Figure 14. Furthermore, the difference between the lower two branches and upper two branches of Figure 17 can be attributed to the restart and NEWT-refinement process described above and displayed in Figure 12. Consequently, the four branches in Figure 17 may represent the potential existence of only one equilibrium branch.

The results obtained for Range 4 are depicted in Figure 18. Again, it is clear that using AUTO for this particular dynamical system does not yield expected results. The numerical instabilities inherent to this problem appear to cause AUTO to diverge from the true equilibrium solutions. Again, it should be noted that the AUTO results are not constant, they only fail to vary at the same rate as in (42). The results shown in Figure 19 were obtained in a similar manner to those of Figure 12, with the discontinuities produced by the restart and NEWT-refinement process described earlier. Each solution composing the line at -10.2° was used as input for NEWT and a refined set of data was obtained. While there were many spurious solutions, just as described with regard to Figure 15, the overwhelming majority of NEWT-refined solutions compared favorably with the interpolated Table 1 data.

Accepting the values obtained in (42) as valid equilibrium solutions, one can see that a number of equilibrium attitude orientations may now be possible. Figure 20 depicts

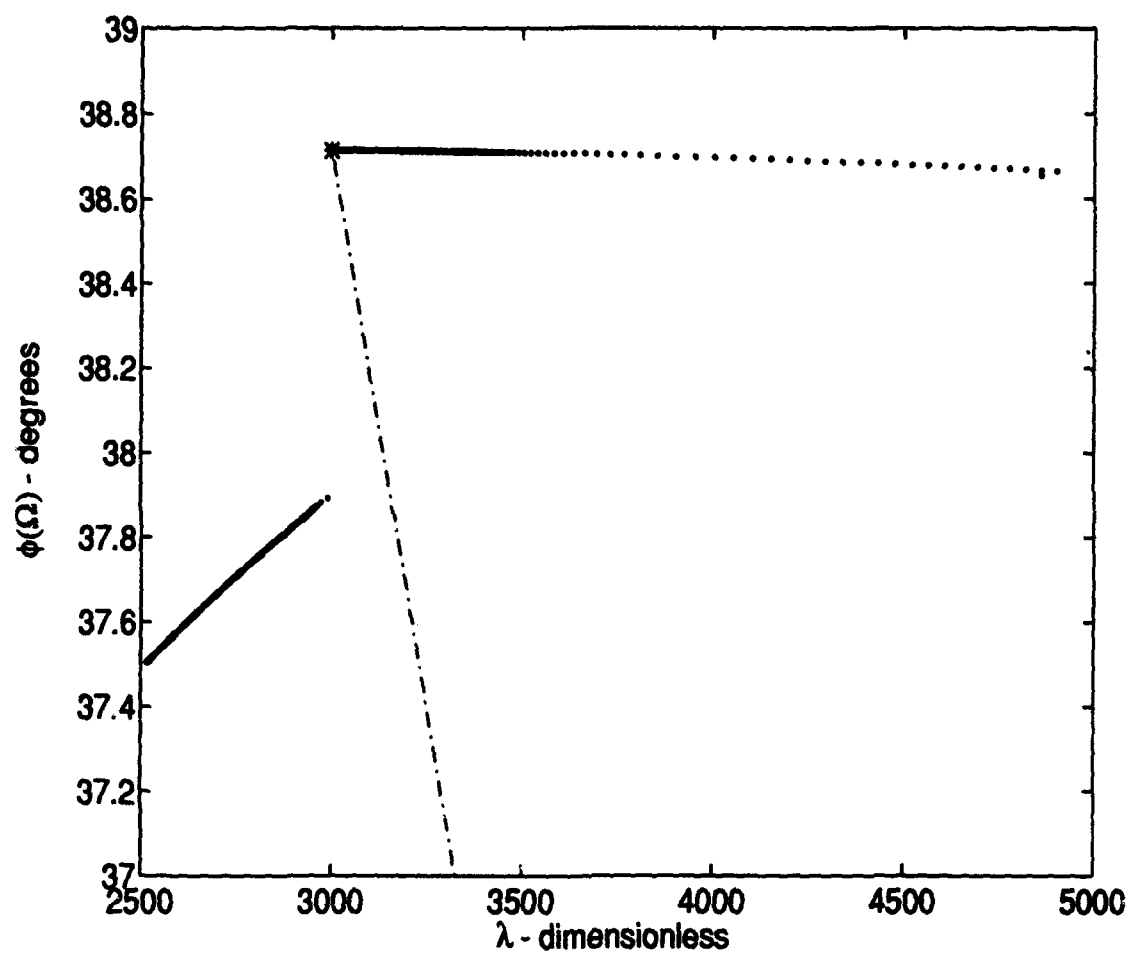


Figure 14. Additional AUTO results in Ranges 2 and 3 are depicted by dots while interpolated data from Table 1 is shown by a dash-dot line.

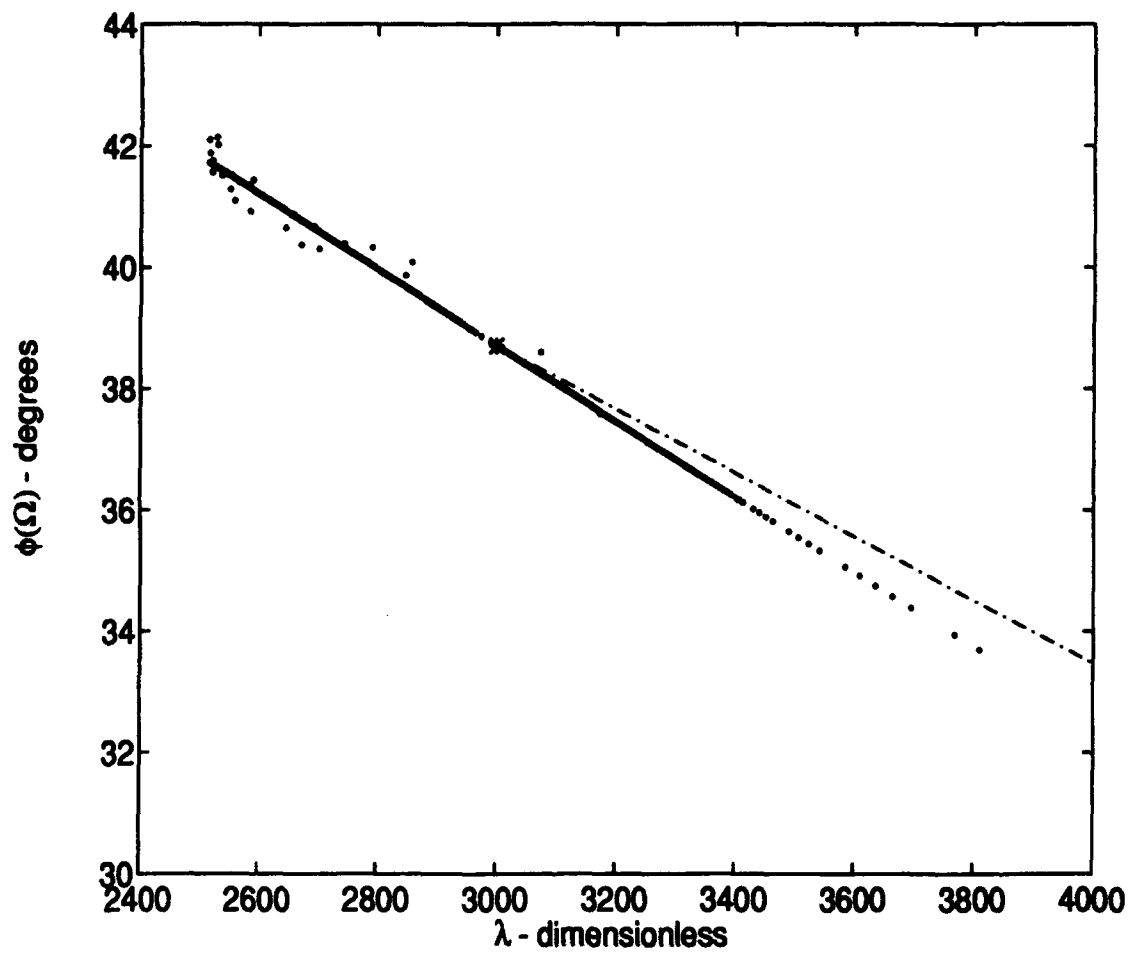


Figure 15. AUTO results in Ranges 2 and 3 refined by NEWT are depicted by dots while interpolated data from Table 1 is shown by a dash-dot line.

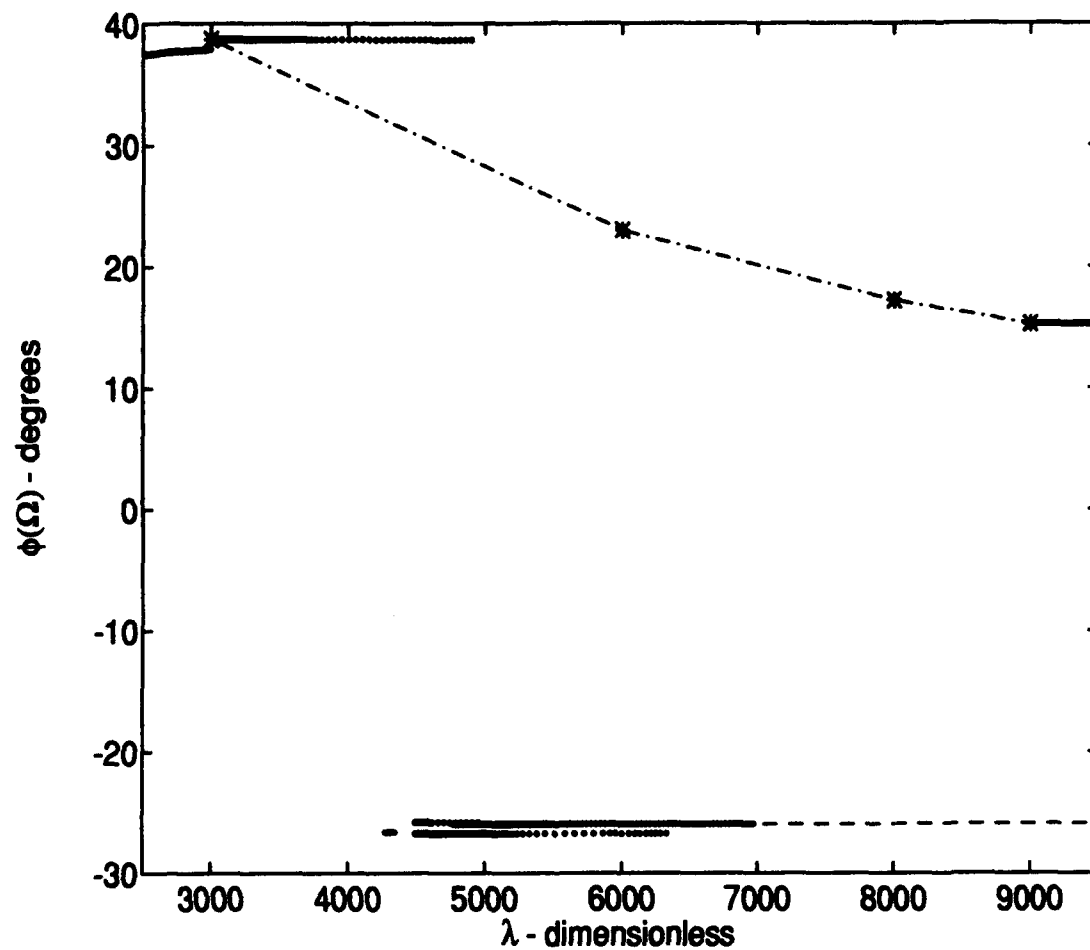


Figure 16. AUTO results in Range 3 are depicted by dots while interpolated data from Table 1 is shown by a dash-dot line.

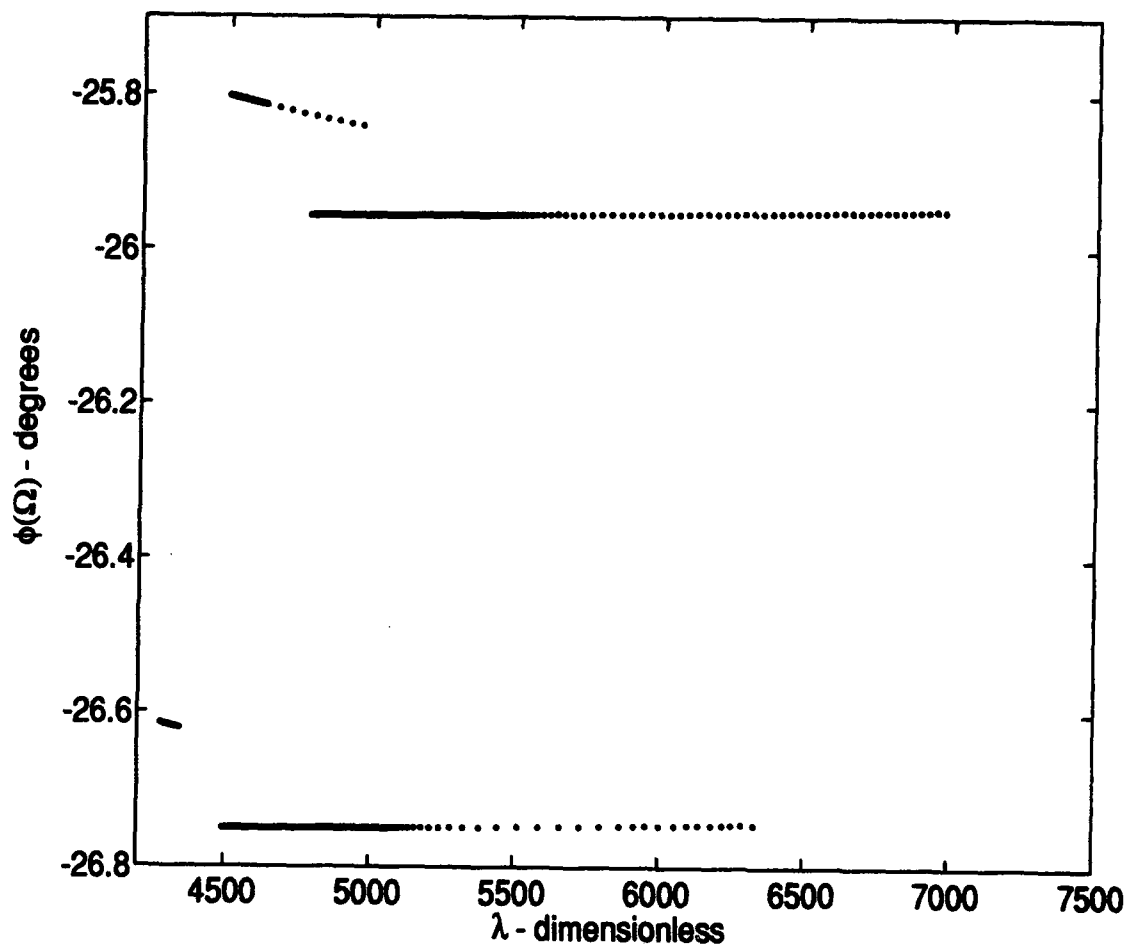


Figure 17. Enlarged view of lower portion of Figure 16. AUTO results in Range 3 are depicted by dots while interpolated data from Table 1 is shown by a dash-dot line.

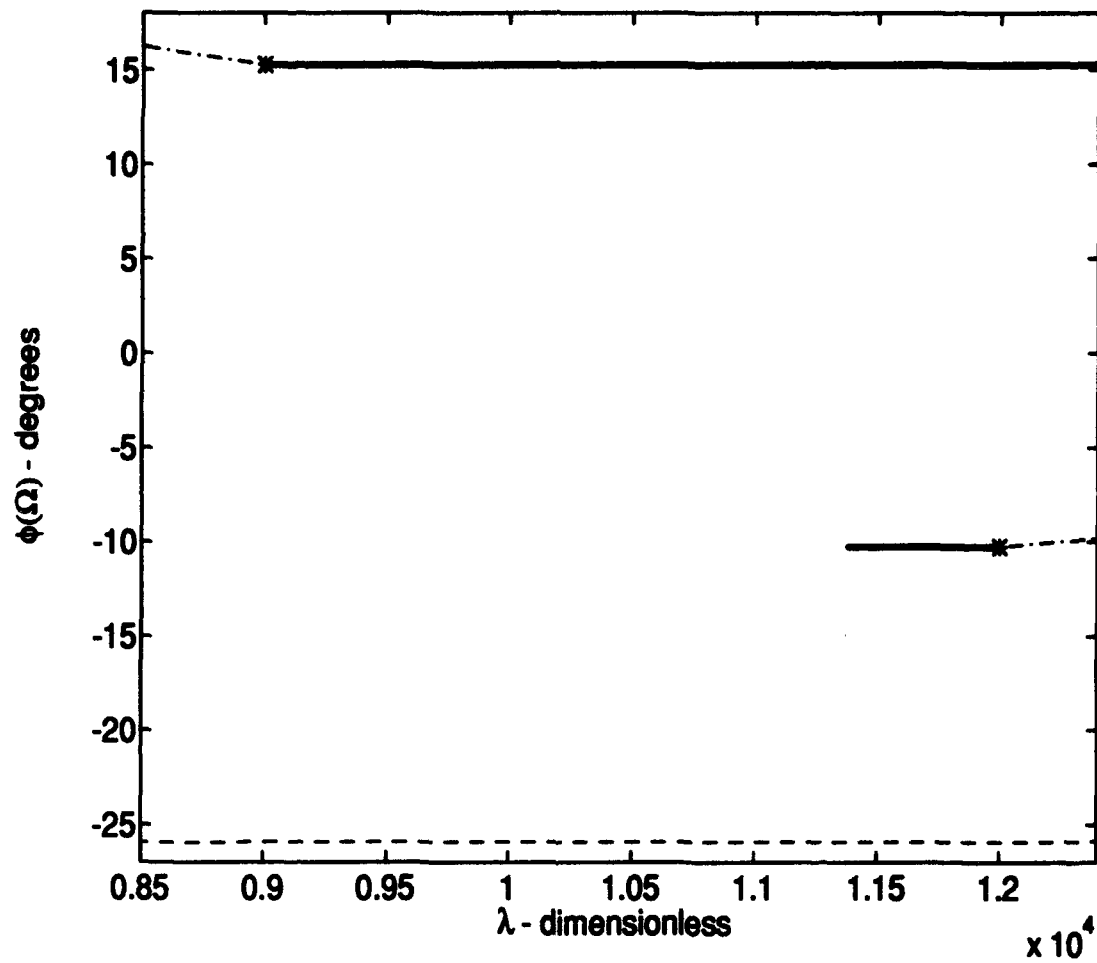


Figure 18. AUTO results in Range 4 are depicted by dots while interpolated data from Table 1 is shown by a dash-dot line.

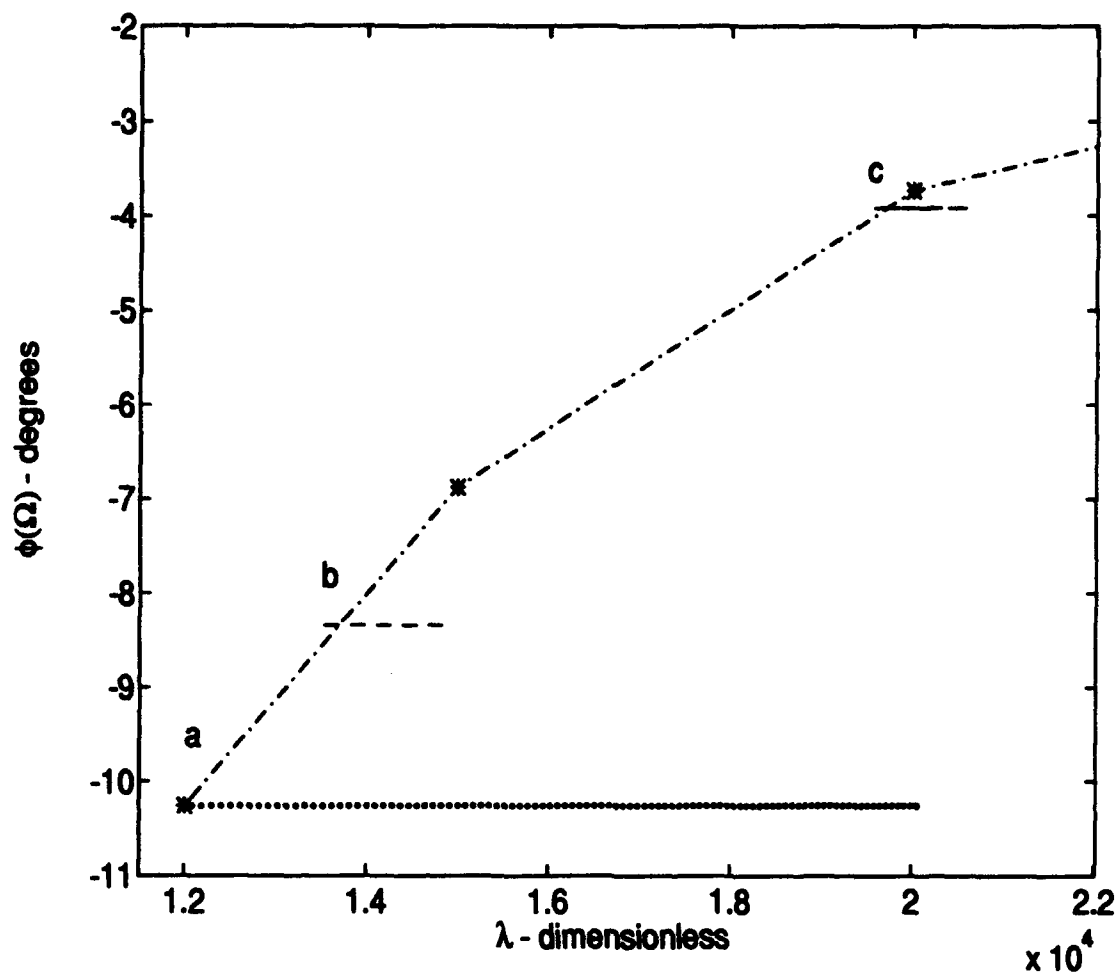


Figure 19. AUTO results in Range 5 are depicted by dots while interpolated data from Table 1 is shown by a dash-dot line. These solutions were obtained by starting with point a, which corresponds to Solution 8. Discontinuities present at points b and c were the result of restart difficulties and the NEWT-refinement process.

a typical gravity-gradient orientation, as well as the three general attitudes indicated in Table 1. The molecule model is not to scale, but representative of the asymmetrical model used for this study. With the center of the gravitational body located vertically down, the three non-great circle orientations are distinctly different from the typical gravity-gradient configuration. These equilibrium attitudes clearly indicate new possibilities for future satellite design.

5.3 Modifications to Improve AUTO

Modifications were made to the AUTO software itself to enhance its performance for this particular dynamical system. Since the Cray did not support a complex double precision eigenvalue solver, AUTO subroutines were modified to take advantage of the symmetric Jacobian in this system. The symmetric Jacobian ensured real rather than complex eigenvalues, thus a complex double precision eigenvalue solver was unnecessary.

Numerical instabilities observed later in the study prompted the use of a singular value decomposition (SVD) rather than gaussian elimination subroutine to solve the system of equations. It was believed that the robust SVD method would eliminate some of the problems addressed in Section 5.5. Although accuracy was improved, as indicated by the Kantorovich variables in Equations 58, the SVD subroutine produced nearly identical solutions to those obtained with the gaussian elimination subroutine.

In order to achieve results as close as possible to those found in (42), an additional convergence test was placed in AUTO to ensure the desired accuracy of solutions. As described in Section 4.4, in order to satisfy the Kantorovich Theorem conditions, γ , the maximum value of δu , was required to be sufficiently small. While AUTO's convergence tests, shown in Equation 57, were being satisfied and implied accurate results, frequently the Kantorovich conditions were not met. One measure of effectiveness observed was the norm of f , which should be a very small number since the goal of the program was to find successive solutions to $f(\lambda, \Omega, \beta) = 0$. The value of f_{norm} obtained with AUTO was not as small as that achieved by using NEWT. Therefore, an additional restriction was added to the acceptance criteria for AUTO-derived equilibrium solutions. Additional iterations were the result if γ was not sufficiently small. As expected, processing time increased

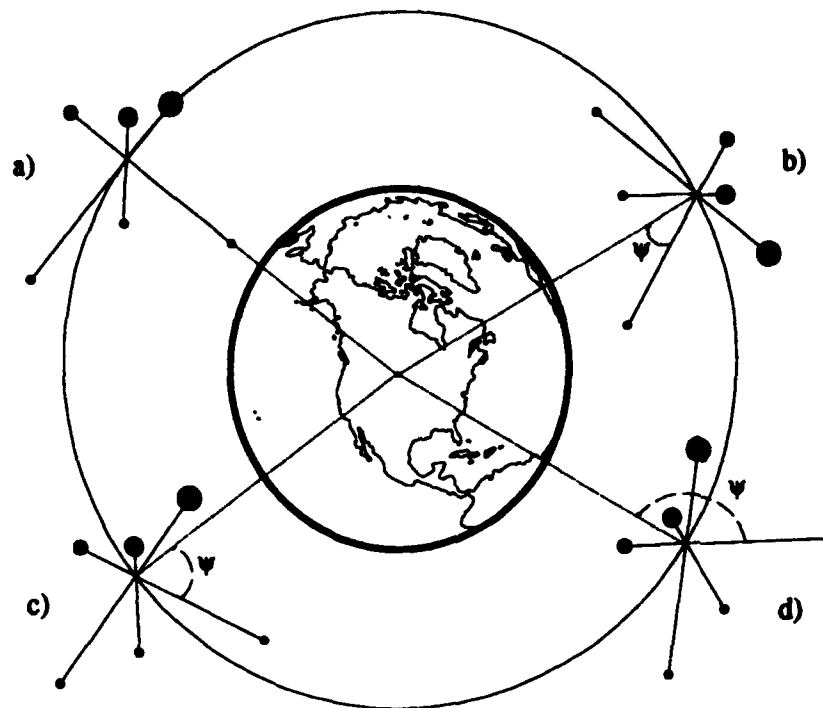


Figure 20. Some non-great circle orbit equilibrium orientations: a) depicts a typical gravity-gradient attitude while b), c), and d) show attitudes representing Solutions 1, 7, and 8 respectively.

and smaller values of f_{norm} were obtained, although still not as small as those achieved in NEWT.

5.4 Additional Steps Toward Efficiency and Accuracy

Given that supercomputer time is not without cost, several attempts were made at finding methods to reduce Cray processing time. In order to ascertain if use of a supercomputer was absolutely essential, a comparison was made between the Cray results and the Sun SparcStation results. Unfortunately the comparison proved the Cray would indeed be necessary to obtain any worthwhile results. Using the same initial solutions, the values of f_{norm} for one iteration on the Cray and Sun respectively were 0.00001 and 50,000. Likewise, the values of $\alpha\sigma\gamma$ were 0.01 and 6,424 — indicating that few, if any, accurate solutions would be found using the Sun. The AUTO subroutines which define the system of equations to be solved was made as efficient as possible, minimizing calculations and reducing compiling time. The subroutine which computes the value of $f(\lambda, \Omega, \beta)$ may be called over a thousand times *per Euler step*, thus economy of calculation is imperative. In an effort to increase the range of solutions obtained in a given number of steps, the variable λ was considered to be the parameter rather than c . However, this approach was abandoned since the associated Jacobian would then become asymmetrical, causing significant problems with the eigenvalue solver as described in Section 5.3.

Furthermore, several scaling schemes were tried after expected results were not obtained. It was realized late in the study that AUTO actually solves the 8×8 matrix formed from Equations 55 and 56. The prior assumption was that only the 7×7 matrix indicated in Equations 39-41 and 55 was analyzed in AUTO. Additionally, because the value of $u(7)$ or β is not part of AUTO's output, it was not initially obvious that the values of $u(1) - u(7)$ ranged significantly in magnitude. For these reasons, efforts were made to scale the 7 initial values, then the Jacobian, and finally the value of the function $f(\lambda, \Omega, \beta)$. Attempts to obtain convergence with AUTO following the scaling modifications were unsuccessful.

5.5 Problems Encountered

The most identifiable problem was an inability to obtain solutions over a large range in a reasonable amount of CPU time. In order to acquire solutions with sufficient accuracy in AUTO, the stepsize had to be made so small that the computational time required to find solutions was entirely too excessive. For example, achieving a continuation from $\lambda = 100$ to 103.9 required over 15 minutes of CPU time on the Cray. Clearly, pursuing this investigative route would have been impractical. In order to fully utilize AUTO's capabilities, further "fine-tuning" of the equilibrium equations in the subroutines is required.

Acquiring a suitable stepsize for use in AUTO also presented significant problems. A number of variables in AUTO may be adjusted by the user to achieve varying degrees of efficiency and accuracy: mesh sizes; initial, minimum, and maximum stepsizes; maximum number of newton iterations; and tolerances — almost a dozen altogether. The results were extremely sensitive to changes in these factors. Several hundred combinations of these variables were used in a trial and error procedure throughout the course of this study in an attempt to find an efficient method of achieving results. Many tradeoffs were made between the variables, as decreasing a tolerance might increase the accuracy but would also prevent initial convergence on the second solution or cause a CPU time limit to be exceeded.

Another idiosyncrasy observed during this particular application of AUTO was discovered while attempting to increase the stepsize. An effective measure of success was obtained by comparing the parameter increase in two runs of the same number of steps. During this process it was noted that different results were achieved depending on how often the data was printed to the screen. The value of the tenth calculated solution obtained by executing 20 steps and printing each one was greater than the value of the tenth calculated solution obtained by executing 20 steps and printing every other solution. The source of this discrepancy was never determined.

Several other puzzling issues arose while employing AUTO. Although a positive stepsize was supposed to cause an increase in the parameter varied by AUTO, the reverse was true for this system of equations. Mathematically this appears impossible, but the intricacy

cies of this unique system of equations combined with AUTO's algorithms appear to have caused this anomaly. Additionally, although AUTO has the capability to restart using an initial value obtained from any portion of a previously obtained equilibrium branch, in this case the feature was successful only sporadically. This presented a significant challenge since the numerical instabilities in the problem caused program execution to terminate prematurely numerous times due to computer processing time-limit violations. The numerical instabilities themselves may also be the cause of the restart problem. Without a functioning restart capability, an alternative avenue for continuing the branch was required.

Possible causes for the restart problem were analyzed. It was speculated that the initial solution provided to AUTO was not of sufficient accuracy to create a valid equilibrium branch with which the restart option would work. Consequently, the conversion of initial states from Table 1 was recalculated in double precision on the Cray and also refined using NEWT, once it was apparent that using double precision did not solve the problem. This technique was moderately successful in achieving better results. However, the restart problem persisted and the refinement process was extended to include the last equilibrium solution determined by AUTO, as well as the initial solution. The presumption was that AUTO had strayed too far from the actual equilibrium branch and was unable to converge on a subsequent solution. Occasionally the refinement process worked, but often NEWT was unable to converge on a nearby solution — the program either failed completely or provided a solution very different from the initial equilibrium solution. Steps were then taken to retain a certain number of AUTO solutions in double precision (29 significant digits) as possible restart values. AUTO, as written, only retains solutions with 10 significant digits for use in subsequent restarts. Unfortunately, this method was also only occasionally effective. Another possible cause for the restart problem is that the states were extremely close to one another and the minuscule variation in those states indicated a bifurcation point to AUTO, preventing a successful restart. As mentioned earlier, a likely explanation for the restart problem concerns the numerical instabilities associated with these equilibrium equations and the large number of significant digits required. The most apparent solution to this problem, keeping these results independent of those of NEWT and (42),

would involve program execution for hundreds of thousands of steps and require the use of batch files. Due to limited computer time, this approach was regarded as unwise.

VI. Conclusions

6.1 Summary

Selected results from (42) were verified, thereby confirming the existence of non-great circle relative equilibria for a rigid body travelling in a central gravitational field. Solutions were obtained utilizing AUTO86, a continuation/bifurcation software package. Anticipated bifurcation points and limit points were not found, presumably due to numerical sensitivity and instabilities present when employing AUTO to analyze this particular dynamical system. Using AUTO and NEWT, a similar program implemented in (42), values and trends of equilibrium solutions were nearly identical to those obtained in (42). Extensive execution of the AUTO program and the current subroutines associated with this system could possibly duplicate and elaborate upon the complete results of (42), however this was not attempted due to prohibitive computational processing time. It is believed that modification of the current subroutines may lead to a more efficient approach and thus more definitive results.

6.2 Operational Significance

The utilization of relative equilibria in non-great circle orbits holds significant potential for both current and future satellites. Current spacecraft are subject to attitude control restrictions based on the classic gravity-gradient model. Greater natural attitude stability for those satellites with active stabilization systems occupying non-great circle orientations can increase pointing stability and accuracy. These satellites would require less artificial or active attitude control and reduce attitude perturbations inherent in artificial means (15). Missions might be expanded without suffering a significant loss in pointing accuracy. Satellites employing a mass expulsion stabilization system could achieve and sustain additional and more complex attitudes naturally, thus reducing propellant required for attitude control and increasing the spacecraft's operational lifetime. Small space test spacecraft with limited lifetimes of days or months might profit considerably, since these types of satellites would not likely have complex active stabilization systems onboard. They might rely instead on an expanded range of stable attitudes caused by gravitational

torques. A three-axis-stabilized spacecraft may have been designed for one set of equilibrium points but may now be modified to operate in a new range of equilibrium points. More importantly, prior knowledge and incorporation of the additional range of stable attitudes would aid engineers in designing satellites with enhanced performance. Reduced station-keeping propellant, greater maneuverability, and longer lifetimes could be realized. Throughout the design phase, new attitudes and configurations could be considered in planning experiments without sacrificing payload requirements.

The missions which might employ non-great circle relative equilibria range from astronomy, space test experiments, and space-based radar, to remote sensing, surveillance, and reconnaissance. Non-great circle relative equilibria could be useful for stellar mapping in the infrared and visible wavelengths. The instrument could be placed in a sun-synchronous orbit with its major axis pointed away from the sun and the natural gravitational torque could be used for passive attitude stabilization (16). For example, although the 11,400-kg Hubble Space Telescope is in a 28.45°-inclination, 610-km orbit as a result of shuttle payload and launch constraints, a more ideal orbit would have been sun-synchronous (37), (34), (3), (16). The current orbit allows stellar observations for only a portion of the orbit — that part in which the earth sufficiently obscures the sun's rays — considerably decreasing useful observation time. A sun-synchronous orbit utilizing these new relative equilibria for attitude stabilization might permit continuous coverage of deep space. Of course, in order for a similar deep space telescope to reach this orbit, an alternative to the shuttle would be required for launch and deployment.

Further examination of non-great circle relative equilibria could possibly explain anomalous behavior of current gravity-gradient satellites, providing that eccentricity, geopotential, thermal, and atmospheric effects have already been eliminated as potential causes. A spacecraft exhibiting unexplained motion away from the classical gravity-gradient attitude may actually be drifting toward these new equilibrium points. While it is typically thought that classic gravity-gradient orientation subjects a spacecraft to a zero overall gravitational torque load, perhaps residual torque exists and the vehicle is inclined to shift toward an attitude of zero load. Proof of this concept would then necessitate modification to Figure 4. While the figure indicates that a satellite at 25,228 km ($10^{4.4}$ km) experiences

a gravitational torque of 8.1721×10^{-5} N-m if at an orientation 8.1721° from the vertical, an orientation obtained from Solution 11 of Table 1, the satellite may actually be in a state of relative equilibrium and thus experiencing zero net gravitational torque.

A major benefit to non-great circle relative equilibria is yaw control. As discussed in Section 2.3, gravitational torques have little influence on motion about the vertical or yaw axis. However, in a non-great circle orbit the off-axis directions of the radius and angular velocity vectors prescribe a specific orientation for an asymmetric satellite, thus possibly improving yaw control.

Unfortunately, despite the utility of non-great circle orbits, it is doubtful that any onboard satellite computer or ground-generated command signals would be capable of maintaining one of the relative equilibrium attitudes described in this study. A current estimate of attitude pointing accuracy is placed at one arcsecond (16). Translated into significant digits of attitude coordinates this would equate to six orders of magnitude — considerably fewer than the 29 significant digits seemingly required by a supercomputer to locate the equilibrium points. Clearly, a more accurate control system would be necessary to take advantage of these newly-found equilibria. However, there is some consolation in noting that at present, this represents a technological challenge rather than an obstacle imposed by the laws of nature.

6.3 Recommendations

Undoubtedly, this subject requires further investigation. It appears that, in this particular case, employing AUTO to trace equilibrium branches and locate bifurcation and limit points is not an uncomplicated task. Two potential courses of action are recommended with regard to AUTO. First, a thorough investigation of the AUTO code for identifiable sensitivities in double precision is suggested. Particular attention should be given to insuring that all constants are defined in double precision. Closer examination of the code in (42) may be required in order to decipher the calculations used to determine the value of the function $f(u)$. Subtle differences in mathematical expressions for *sum* may have lead to discrepancies between the codes used in this study and in (42). Additional examination of the use of the SVD subroutine is also suggested. Apparently, in NEWT's

application of SVD, the small elements of the diagonal matrix W , the "small $w(j)$'s," are not zeroed as is advised in (27:55-56). Further experimentation with changes in mesh parameters (NTST and NCOL) is also advised. Most importantly, a suitable scaling scheme must be developed in order to improve program efficiency. Given finite computational and economical resources, the scaling issue is critical. The satellite model could also be changed to reduce the asymmetrical characteristics which magnify the numerical instabilities present in the problem. Second, if the first course of action is futile, use of an alternate continuation code is recommended.

Once the results of (42) are extensively validated, whether through AUTO or an original program, the equations of equilibrium should be analyzed for a solid body which more closely resembles an orbiting vehicle. One potential candidate is the NRL-164 (5). Accomplishment of this objective would further establish potential applications to real satellites and be a prelude to full-scale development and operational use of spacecraft employing non-great circle relative equilibria.

Appendix A. AUTO Subroutines

This appendix contains the mathematical expressions used in creating the AUTO subroutines for this thesis. The associated code is also included.

The vector form of Equations 39-41 was converted into scalar form as follows:

$$f_1 = (\Omega_1^2 + \Omega_2^2 + \Omega_3^2)\lambda_1 - (\Omega_1\lambda_1 + \Omega_2\lambda_2 + \Omega_3\lambda_3)\Omega_1 - A \text{ sum}_1 \quad (59)$$

$$f_2 = (\Omega_1^2 + \Omega_2^2 + \Omega_3^2)\lambda_2 - (\Omega_1\lambda_1 + \Omega_2\lambda_2 + \Omega_3\lambda_3)\Omega_2 - A \text{ sum}_2 \quad (60)$$

$$f_3 = (\Omega_1^2 + \Omega_2^2 + \Omega_3^2)\lambda_3 - (\Omega_1\lambda_1 + \Omega_2\lambda_2 + \Omega_3\lambda_3)\Omega_3 - A \text{ sum}_3 \quad (61)$$

$$f_4 = I_{11}\Omega_1 + (\lambda_1^2 + \lambda_2^2 + \lambda_3^2)\Omega_1 - (\Omega_1\lambda_1 + \Omega_2\lambda_2 + \Omega_3\lambda_3)\lambda_1 + \beta\Omega_1 \quad (62)$$

$$f_5 = I_{22}\Omega_2 + (\lambda_1^2 + \lambda_2^2 + \lambda_3^2)\Omega_2 - (\Omega_1\lambda_1 + \Omega_2\lambda_2 + \Omega_3\lambda_3)\lambda_2 + \beta\Omega_2 \quad (63)$$

$$f_6 = I_{33}\Omega_3 + (\lambda_1^2 + \lambda_2^2 + \lambda_3^2)\Omega_3 - (\Omega_1\lambda_1 + \Omega_2\lambda_2 + \Omega_3\lambda_3)\lambda_3 + \beta\Omega_3 \quad (64)$$

$$f_7 = \frac{1}{2}(\Omega_1^2 + \Omega_2^2 + \Omega_3^2) - c \quad (65)$$

where

$$\begin{aligned} \text{sum}_1 &= \frac{m_1[\lambda_1 + Q_1(1)]}{[(\lambda_1 + Q_1(1))^2 + (\lambda_2 + Q_1(2))^2 + (\lambda_3 + Q_1(3))^2]^{\frac{3}{2}}} \\ &+ \frac{m_2[\lambda_1 + Q_2(1)]}{[(\lambda_1 + Q_2(1))^2 + (\lambda_2 + Q_2(2))^2 + (\lambda_3 + Q_2(3))^2]^{\frac{3}{2}}} \\ &+ \frac{m_3[\lambda_1 + Q_3(1)]}{[(\lambda_1 + Q_3(1))^2 + (\lambda_2 + Q_3(2))^2 + (\lambda_3 + Q_3(3))^2]^{\frac{3}{2}}} \\ &+ \frac{m_4[\lambda_1 + Q_4(1)]}{[(\lambda_1 + Q_4(1))^2 + (\lambda_2 + Q_4(2))^2 + (\lambda_3 + Q_4(3))^2]^{\frac{3}{2}}} \\ &+ \frac{m_5[\lambda_1 + Q_5(1)]}{[(\lambda_1 + Q_5(1))^2 + (\lambda_2 + Q_5(2))^2 + (\lambda_3 + Q_5(3))^2]^{\frac{3}{2}}} \\ &+ \frac{m_6[\lambda_1 + Q_6(1)]}{[(\lambda_1 + Q_6(1))^2 + (\lambda_2 + Q_6(2))^2 + (\lambda_3 + Q_6(3))^2]^{\frac{3}{2}}} \\ \text{sum}_2 &= \frac{m_1[\lambda_2 + Q_1(2)]}{[(\lambda_1 + Q_1(1))^2 + (\lambda_2 + Q_1(2))^2 + (\lambda_3 + Q_1(3))^2]^{\frac{3}{2}}} \\ &+ \frac{m_2[\lambda_2 + Q_2(2)]}{[(\lambda_1 + Q_2(1))^2 + (\lambda_2 + Q_2(2))^2 + (\lambda_3 + Q_2(3))^2]^{\frac{3}{2}}} \\ &+ \frac{m_3[\lambda_2 + Q_3(2)]}{[(\lambda_1 + Q_3(1))^2 + (\lambda_2 + Q_3(2))^2 + (\lambda_3 + Q_3(3))^2]^{\frac{3}{2}}} \\ &+ \frac{m_4[\lambda_2 + Q_4(2)]}{[(\lambda_1 + Q_4(1))^2 + (\lambda_2 + Q_4(2))^2 + (\lambda_3 + Q_4(3))^2]^{\frac{3}{2}}} \end{aligned} \quad (66)$$

$$\begin{aligned}
& + \frac{m_5[\lambda_2 + Q_5(2)]}{[(\lambda_1 + Q_5(1))^2 + (\lambda_2 + Q_5(2))^2 + (\lambda_3 + Q_5(3))^2]^{\frac{3}{2}}} \\
& + \frac{m_6[\lambda_2 + Q_6(2)]}{[(\lambda_1 + Q_6(1))^2 + (\lambda_2 + Q_6(2))^2 + (\lambda_3 + Q_6(3))^2]^{\frac{3}{2}}} \quad (67) \\
sum_3 = & \frac{m_1[\lambda_3 + Q_1(3)]}{[(\lambda_1 + Q_1(1))^2 + (\lambda_2 + Q_1(2))^2 + (\lambda_3 + Q_1(3))^2]^{\frac{3}{2}}} \\
& + \frac{m_2[\lambda_3 + Q_2(3)]}{[(\lambda_1 + Q_2(1))^2 + (\lambda_2 + Q_2(2))^2 + (\lambda_3 + Q_2(3))^2]^{\frac{3}{2}}} \\
& + \frac{m_3[\lambda_3 + Q_3(3)]}{[(\lambda_1 + Q_3(1))^2 + (\lambda_2 + Q_3(2))^2 + (\lambda_3 + Q_3(3))^2]^{\frac{3}{2}}} \\
& + \frac{m_4[\lambda_3 + Q_4(3)]}{[(\lambda_1 + Q_4(1))^2 + (\lambda_2 + Q_4(2))^2 + (\lambda_3 + Q_4(3))^2]^{\frac{3}{2}}} \\
& + \frac{m_5[\lambda_3 + Q_5(3)]}{[(\lambda_1 + Q_5(1))^2 + (\lambda_2 + Q_5(2))^2 + (\lambda_3 + Q_5(3))^2]^{\frac{3}{2}}} \\
& + \frac{m_6[\lambda_3 + Q_6(3)]}{[(\lambda_1 + Q_6(1))^2 + (\lambda_2 + Q_6(2))^2 + (\lambda_3 + Q_6(3))^2]^{\frac{3}{2}}} \quad (68)
\end{aligned}$$

The Jacobian, $f'(\lambda, \Omega, \beta)$, of Equations 39-41 was also required to perform the numerical analysis of the equations of equilibrium. The Jacobian may be expressed as

$$\left[f'(\lambda, \Omega, \beta) \right] = \begin{bmatrix} \left\{ (|\Omega|^2 - \sum_{i=1}^6 \frac{Am_i}{|\lambda + Q_i|^3}) 1 - \Omega\Omega^T - (\lambda \cdot \Omega)1 + 2\lambda\Omega^T - \Omega\lambda^T \right. & 0 \\ \left. + \sum_{i=1}^6 \frac{3Am_i}{|\lambda + Q_i|^5} (\lambda + Q_i)(\lambda + Q_i)^T \right\} & \\ -(\lambda \cdot \Omega)1 + 2\lambda\Omega^T - \Omega\lambda^T & \mathbf{I} + (|\lambda|^2 - \beta)1 - \lambda\lambda^T & -\Omega \\ 0 & -\Omega & 0 \end{bmatrix} \quad (69)$$

where the vector, rather than component, form is used in the interest of simplicity.

The following pages contain a listing of applicable subroutines used in AUTO for this particular dynamical system. However, the SVD subroutines are not included since they are copyrighted in (27).


```

      SUBROUTINE FUNC(NDIM,U,ICP,PAR,IJAC,F,DFDU,DFDP)
      -----
C
C
C This subroutine evaluates the right hand side of the first order
C system and the derivatives with respect to (U(1),U(2))
C and with respect to the free parameters.
C
C Input parameters :
C   NDIM   -   Dimension of U and F.
C   U       -   Vector containing U.
C   PAR     -   Array of parameters in the differential equations.
C   ICP     -   PAR(ICP(1)) is the initial 'free' parameter.
C               PAR(ICP(2)) is a secondary 'free' parameter,
C               for subsequent 2-parameter continuations.
C   IJAC    -   =1 if the Jacobians DFDU and DFDP are to be returned,
C               =0 if only F(U,PAR) is to be returned in this call.
C
C Values to be returned :
C   F       -   F(U,PAR) the right hand side of the ODE.
C   DFDU    -   The derivative (Jacobian) with respect to U.
C               DFDU(i,j) must be given the value of  $d F(i) / d U(j)$  .
C
C   DFDP    -   The derivative with respect to the 'free' parameters:
C               DFDP(i,ICP(j)) =  $d F(i) / d PAR(ICP(j))$ .
C
      IMPLICIT DOUBLE PRECISION (A-H,O-Z)
      CSGL REAL (A-H,O-Z)
C
      COMMON /ERRAN/ GAMMA, ALAMDA, SIGMAE, ALPHA, RHOMIN,FNORM

      DOUBLE PRECISION U(NDIM),PAR(20)
      DOUBLE PRECISION F(NDIM),DFDU(NDIM,NDIM),DFDP(NDIM,20)
      DOUBLE PRECISION In(3,3),m(6),mag2lQ(6),lam2,num
      DOUBLE PRECISION sum(3),dsdl(3,3),Q(6,3)
      INTEGER I,J

C   DATA STATEMENTS
      DATA ((dsdl(i,j),i=1,3),j=1,3)/9 * 0.0/
      DATA ((In(i,j),j=1,3),i=1,3)/.3332,0,0,0,.3335,0,0,0,.3333/
      DATA ((Q(i,j),j=1,3),i=1,6)/18*0.0/
      DATA (m(i),i=1,6)/0.330066d+0,0.00330033d+0,0.330033d+0,
      +0.00330033d+0,0.33d+0,0.00330034d+0/

C
      Q(1,1) = 7.0731919616600413122865203958d-2

```

```

Q(2,1) = -7.0738992101313602961134447941d+0
Q(3,2) = 7.0675314289714873863597724646d-2
Q(4,2) = -7.0675314289714838201090703958d+0
Q(5,3) = 7.072489203617885186701998299d-2
Q(6,3) = -7.0717605979820975582255668867d+0

```

C***** Useful quantities *****

```

om2 = u(4)**2+u(5)**2+u(6)**2
omdlam = u(4)*u(1)+u(5)*u(2)+u(6)*u(3)
lam2=u(1)**2 + u(2)**2 + u(3)**2
A=0.04*(sqrt(lam2))**5

```

C***** Calculating the sum *****

```

do 10 j=1,3
  sum(j)=0.0
  do 20 i=1,6
    num=m(i)*(u(j)+Q(i,j))
    mag2lQ(i)=(u(1)+Q(i,1))**2+(u(2)+Q(i,2))**2 +
      (u(3)+Q(i,3))**2
    den=sqrt(mag2lQ(i)**3)
    sum(j)=sum(j)+num/den
  20 continue
10 continue

```

C***** Calculating F *****

```

do 30 j=1,3
  F(j)=om2*u(j)-omdlam*u(j+3)-A*sum(j)
  F(j+3)=(In(j,1)*u(4))+(In(j,2)*u(5))+(In(j,3)*u(6))+
    (lam2*u(j+3)) -(omdlam*u(j))+(u(7)*u(j+3))
30 continue
F(7)=.5*om2-par(1)
fnorm=F(1)**2+F(2)**2+F(3)**2+F(4)**2+F(5)**2+F(6)**2
  +F(7)**2
fnorm=sqrt(fnorm)
C  write(6,*) 'fnorm=',fnorm

```

IF(IJAC.EQ.0)RETURN

C

C ***** Calculating the partials of sum() with respect to
C lambda(1,2,3)

C

```

DO 25 I=1,3
  dsdl(i,i)=dsdl(i,i) + (m(j)*(mag2lQ(j))**(-1.5)) - 3.0 *

```

```

      m(j) * (mag21q(j))**(-2.5)*(u(i)+q(j,i))**2
25  Continue
      dsdl(1,2)=dsdl(1,2) -3.0*(m(j)*(mag21q(j))**(-2.5)) *
      (u(1)+q(j,1))*(u(2)+q(j,2))
      dsdl(1,3)=dsdl(1,3) -3.0*(m(j)*(mag21q(j))**(-2.5)) *
      (u(1)+q(j,1))*(u(3)+q(j,3))
      dsdl(2,3)=dsdl(2,3) -3.0*(m(j)*(mag21q(j))**(-2.5)) *
      (u(2)+q(j,2))*(u(3)+q(j,3))
26  Continue
      dsdl(2,1)=dsdl(1,2)
      dsdl(3,1)=dsdl(1,3)
      dsdl(3,2)=dsdl(2,3)

```

C Derivatives of F() with respect to U()

C

```

DFDU(1,1)= u(5)**2+u(6)**2 - A*dsdl(1,1)
DFDU(1,2)= -u(4)*u(5) - A*dsdl(1,2)
DFDU(1,3)= -u(4)*u(6) - A*dsdl(1,3)
DFDU(1,4)= -u(5)*u(2) - u(6)*u(3)
DFDU(1,5)= 2.0*u(5)*u(1) - u(4)*u(2)
DFDU(1,6)= 2.0*u(6)*u(1) - u(4)*u(3)
DFDU(1,7)= 0.0
DFDU(2,1)= -u(4)*u(5)-A*dsdl(2,1)
DFDU(2,2)= u(4)**2 + u(6)**2 - A*dsdl(2,2)
DFDU(2,3)= -u(5)*u(6) - A*dsdl(2,3)
DFDU(2,4)= 2.0*u(4)*u(2) - u(5)*u(1)
DFDU(2,5)= -u(4)*u(1) - u(6)*u(3)
DFDU(2,6)= 2.0*u(6)*u(2) - u(5)*u(3)
DFDU(2,7)= 0.0
DFDU(3,1)= -u(4)*u(6) - A*dsdl(3,1)
DFDU(3,2)= -u(5)*u(6) - A*dsdl(3,2)
DFDU(3,3)= u(4)**2 + u(5)**2 - A*dsdl(3,3)
DFDU(3,4)= 2*u(4)*u(3) - u(6)*u(1)
DFDU(3,5)= 2*u(5)*u(3) - u(6)*u(2)
DFDU(3,6)= -u(4)*u(1) - u(5)*u(2)
DFDU(3,7)= 0.0
DFDU(4,1)= DFDU(1,4)
DFDU(4,2)= DFDU(2,4)
DFDU(4,3)= DFDU(3,4)
DFDU(4,4)= In(1,1)+u(2)**2 + u(3)**2 + u(7)
DFDU(4,5)= In(1,2)-u(2)*u(1)
DFDU(4,6)= In(1,3)-u(3)*u(1)
DFDU(4,7)= u(4)
DFDU(5,1)= DFDU(1,5)
DFDU(5,2)= DFDU(2,5)

```

```

DFDU(5,3)= DFDU(3,5)
DFDU(5,4)= In(2,1)-u(1)*u(2)
DFDU(5,5)= In(2,2)+u(1)**2+u(3)**2 + u(7)
DFDU(5,6)= In(2,3)-u(3)*u(2)
DFDU(5,7)= u(5)
DFDU(6,1)= DFDU(1,6)
DFDU(6,2)= DFDU(2,6)
DFDU(6,3)= DFDU(3,6)
DFDU(6,4)= In(3,1)-u(1)*u(3)
DFDU(6,5)= In(3,2)-u(2)*u(3)
DFDU(6,6)= In(3,3)+u(1)**2+u(2)**2 + u(7)
DFDU(6,7)= u(6)
DFDU(7,1)= 0.0
DFDU(7,2)= 0.0
DFDU(7,3)= 0.0
DFDU(7,4)= u(4)
DFDU(7,5)= u(5)
DFDU(7,6)= u(6)
DFDU(7,7)= 0.0

C
C Derivatives with respect to PAR(1).
C
    DFDP(1,1)=0.0
    DFDP(2,1)=0.0
    DFDP(3,1)=0.0
    DFDP(4,1)=0.0
    DFDP(5,1)=0.0
    DFDP(6,1)=0.0
    DFDP(7,1)=-1.0

C
    RETURN
    END

C
    SUBROUTINE STPNT(NDIM,U,PAR)
    -----
C
C In this subroutine the steady state starting point must be defined.
C (Used when not restarting from a previously computed solution).
C The problem parameters (PAR) may be initialized here or else in INIT.
C
C     NDIM   -   Dimension of the system of equations.
C     U       -   Vector of dimension NDIM.
C               Upon return U should contain a steady state solution
C               corresponding to the values assigned to PAR.
C     PAR    -   Array of parameters in the differential equations.

```

```

C
C   u.dat is a 6-line input data file consisting of the 3 components
C   of lambda and the 3 components of omega (in cartesian coordinates)
C
      IMPLICIT DOUBLE PRECISION (A-H,O-Z)
CSGLE IMPLICIT REAL (A-H,O-Z)
C
C
      DIMENSION U(NDIM),PAR(20)
      OPEN (UNIT=4, FILE = 'u.dat')
      DO 22 I=1,6
      READ (4,33) U(I)
      write(6,33) u(i)
22  CONTINUE
33  format(D36.30)
      U(7)=- (u(1)**2 + u(2)**2 + u(3)**2)
      par(1)=0.5d0*(u(4)**2+u(5)**2+u(6)**2)
      CLOSE (UNIT = 4)
44  RETURN
      END
C
      SUBROUTINE INIT
C   -----
C
C   In this subroutine the user should set those constants that require
C   values that differ from the default values assigned in DFINIT.
C   (See the main documentation for the default assignments).
C
      IMPLICIT DOUBLE PRECISION (A-H,O-Z)
CSGLE IMPLICIT REAL (A-H,O-Z)
C
      COMMON /BLBCN/ NDIM,IPS,IRS,ILP,ICP(20),PAR(20)
      COMMON /BLCDE/ NTST,NCOL,IAD,ISP,ISW,IPLT,NBC,NINT
      COMMON /BLTHT/ THETA(20), THETAU
      COMMON /BLDLS/ DS,DSMIN,DSMAX,IADS
      COMMON /BLEPS/ EPSL(20),EPSU,EPSS
      COMMON /BLLIM/ NMX,NUZR,RLO,RL1,A0,A1
      COMMON /BLMAX/ NPR,MXBF,IID,ITMX,ITNW,NWTN,JAC
C
      NDIM=7
      IPS=1
      ILP=1
      ISP=2
C
C   Set the principal bifurcation parameter to be PAR(1).

```

```

C      ICP(1)=1
C
C      Set the second free parameter to be PAR(2).
C      (For 2-parameter continuation).
C
C      ICP(2)=2

      MXBF=50
      ITMX=200
      IID=0
      ISW=1
      NUZR=0

      OPEN (UNIT=5, FILE = 'in.dat')
      READ (5,*) IRS
      READ (5,*) NTST
      READ (5,*) NCOL
      READ (5,*) DS
      READ (5,*) DSMIN
      READ (5,*) DSMAX
      READ (5,*) NMX
      READ (5,*) ITNW
      READ (5,*) NPR
      READ (5,*) THETAU
      READ (5,*) THETAL(1)
      READ (5,*) EPSU
      READ (5,*) EPSL(1)
      READ (5,*) EPSS
      READ (5,*) RLO
      READ (5,*) RL1
      READ (5,*) A0
      READ (5,*) A1
      READ (5,*) MXBF
      READ (5,*) ITMX
      READ (5,*) IID

      CLOSE (UNIT=5)

      RETURN
      END
C
C      FUNCTION USZR(I,NUZR,PAR)
C      -----
C

```

```

C This subroutine can be used to obtain plotting and restart data
C at certain values of free parameters.
C
      IMPLICIT DOUBLE PRECISION (A-H,O-Z)
      CSGLE IMPLICIT REAL (A-H,O-Z)
C
      DIMENSION PAR(20)
C
C Initially, for the steady state analysis, set NUZR=0 in INIT.
C Then the functions specified below will be ignored.
C
C During the second run of this test problem, when computing the branch
C of periodic solutions, set NUZR=4 in INIT.
C In this example, output will then be written in unit 8 for the values
C of PAR(11) specified below.
C Note that PAR(11) is normally reserved. It is used by AUTO to keep
C track of the period (See main documentation).
C
      GOTO(1,2,3,4)I
C
1      USZR=PAR(11) - 11.0
C      RETURN
C
2      USZR=PAR(11) - 14.0
      RETURN
C
3      USZR=PAR(11) - 20.0
      RETURN
C
4      USZR=PAR(11) - 30.0
      RETURN
C
      END
C
      -----
      SUBROUTINE CAB1(U,DU)
C
      IMPLICIT DOUBLE PRECISION (A-H,O-Z)
      CSGLE IMPLICIT REAL (A-H,O-Z)
C
C determines the max value of DU (or dx) for Kantorovich test
C
      DIMENSION DU(7), U(7)
      COMMON /ERRAN/ GAMMA, ALAMDA, SIGMAE, ALPHA, RHOMIN, FNORM
      GAMMA=0.0d0

```

```

DO 10 I=1,7
  IF(DABS(DU(I)).GT.GAMMA) GAMMA=DABS(DU(I))
10 CONTINUE
  ALAMDA=SQRT(U(1)**2 + U(2)**2 + U(3)**2)
C   WRITE(6,*)'GAMMA = ',GAMMA
  RETURN
END

C   -----
SUBROUTINE CAB2(EV)
C
  IMPLICIT DOUBLE PRECISION (A-H,O-Z)
CSGLE IMPLICIT REAL          (A-H,O-Z)
C
C determines rhomin, sigma, alpha for Kantorovich test
C
  DIMENSION EV(7)
  COMMON /ERRAM/ GAMMA, ALAMDA, SIGMAE, ALPHA, RHOMIN,FNORM
  RHOMIN=1.0d20
  DO 10 I=1,7
  IF(ABS(REAL(EV(I))).LT.RHOMIN) RHOMIN=ABS(REAL(EV(I)))
10 CONTINUE
  SIGMAE = 7.0/RHOMIN
  ALPHA = 2.0* 7.0* ALAMDA
  RETURN
END

C   -----
SUBROUTINE CAB3(RDRLM,DRLM,RL,RDUMX,DUMX,UMX,EPSL,EPSU)
C
  IMPLICIT DOUBLE PRECISION (A-H,O-Z)
CSGLE IMPLICIT REAL          (A-H,O-Z)
C
C compares values with tolerances to determine convergence
C
  DIMENSION RL(20), EPSL(20)
  IF(RDRLM.LE.EPSL(1).AND.RDUMX.LE.EPSU)then
    write(6,*) '(DRLM = ',DABS(DRLM),')'
    write(6,*) '----- = ',RDRLM,' <= ',EPSL(1)
    write(6,*) '1+(RL(1)=',DABS(RL(1)),')'
    write(6,*) '(DUMX = ', DUMX,')'
    write(6,*) '----- = ',RDUMX,' <= ',EPSU
    write(6,*) '1+(UMX=',UMX,')'
  endif
  RETURN

```



```

      END

C      -----
      SUBROUTINE CAB4
C
      IMPLICIT DOUBLE PRECISION (A-H,O-Z)
      CSGLE IMPLICIT REAL          (A-H,O-Z)
C
C prints kantorovich values just prior to convergence
C
      COMMON /ERRAN/ GAMMA, ALAMDA, SIGMAE, ALPHA, RHOMIN, FNORM
      write(6,*) 'Fnorm =          ', fnorm
      WRITE(6,*) 'GAMMA =          ', GAMMA
      WRITE (6,*) 'ALPHA*SIGMA*GAMMA = ', ALPHA*SIGMAE*GAMMA
      IF(ALPHA*SIGMAE*GAMMA.GE.0.5) THEN
      WRITE(6,*) 'ALPHA*SIGMA*GAMMA IS OUT OF BOUNDS *****'
      ENDIF
      RETURN
      END

C      -----
      SUBROUTINE CAB5(NN,M,A,NRHS,NDIMP1,X,NDIMP11,B,IR,IC)
      PA=AMETER (N=8)
C
C NDIMP1 = M1AA = NDIM +1 = 8 FOR cab/wang project
C NDIMP1: number of equations, N
C M1AA: first dimension of A from DIMENSION statement, N
C AA: N * N matrix of coefficients, A
C NRHS number of right hand sides
C NDIMP1: first dimension of U from DIMENSION statement, N
C DU: on exit DU contains the solution vector(s), X
C NDIMP1: first dimension of F from DIMENSION statement, N
C RHS: right hand side vector(s), B
C IR, IC: integer vectors of dimension at least N
C
C The input matrix A is overwritten.

      IMPLICIT DOUBLE PRECISION (A-H,O-Z)
      CSGLE IMPLICIT REAL          (A-H,O-Z)
C
C prepares and calls SVDCMP and SVDBKSB
C
C SVDCMP and SVDBKSB are not included in this code due to copyright laws
C
C in the remaining subroutines U does not imply U the state vector solved

```

```

c in FUNC, this U goes with U, V, W in using SVDcmp
c
      DIMENSION A(N,N),U(N,N),W(N),V(N,N),B(N),X(N)
      DO 20 I=1,N
        DO 10 J=1,N
10          U(I,J) = A(I,J)
20        CONTINUE
      CALL SVDcmp(U,N,N,N,N,W,V)
      WMAX=0.0D0
      DO 13 J=1,N
        IF(W(J).GT.WMAX)WMAX=W(J)
13      CONTINUE
c
C ***** experiment with this value below
c wang's code does not zero the small wj's as advised in "Numerical
C Recipes in Fortran"
c
      write(6,*)'w=',(w(j),j=1,7)
      WMIN=WMAX*1.0D-20
      DO 14 J=1,N
        IF(W(J).LT.WMIN)W(J)=0
14      CONTINUE

      CALL SVBksb(U,W,V,N,N,N,N,B,X)

      RETURN
      END

C -----
      SUBROUTINE CAB6(NTOT,LAB,U)
C
      IMPLICIT DOUBLE PRECISION (A-H,O-Z)
      CSGLT IMPLICIT REAL          (A-H,O-Z)
C
C writes u for interesting or last points to a file
C
      DIMENSION U(7)
      open(unit=11,file='u.last.dat')
      do 10 i=1,6
        write(11,222) u(i)
10      continue
      write(11,*) ntot
222     format(d36.30)
      close(11)

```

RETURN
END

C -----

C

C The following subroutines are not used in this example

C

SUBROUTINE BCND(NDIM,PAR,ICP,NBC,UO,U1,FB,IJAC,DBC)

C -----

RETURN
END

SUBROUTINE ICND(NDIM,PAR,ICP,NINT,U,UOLD,UDOT,UPOLD,FI,IJAC,DINT)

C -----

RETURN
END

SUBROUTINE FOPT(NDIM,U,ICP,PAR,IJAC,FS,DFDU,DFDP)

C -----

RETURN
END

Bibliography

1. Beal, R.T., P.H. Cudmore, R.H. Kronke, and P.G. Wilhelm. "System Performance and Attitude Sensing of Three Gravity-Gradient-Stabilized Satellites," *NASA SP-107 — Symposium on Passive Gravity-Gradient Stabilization*. Washington DC: National Aeronautics and Space Administration, 1966.
2. Chapra, Steven C. and Raymond P. Canale. *Numerical Methods for Engineers*. New York: McGraw-Hill, 1988.
3. Covault, Craig C. "Hubble Returns Good Data But Future Is Clouded," *Aviation Week and Space Technology*: 20-22 (28 October 1991).
4. Doedel, Eusebius J. *AUTO: Software for Continuation and Bifurcation Problems in Ordinary Differential Equations*. Software Users Manual, 1986.
5. Goldman, Robert L. "Influence of Thermal Distortion on Gravity Gradient Stabilization," *Journal of Spacecraft and Rockets*, 12: 406-413 (July 1975).
6. Griffin, Michael D. and James R. French. *Space Vehicle Design*. Washington DC: AIAA, 1991.
7. Hall, Christopher D., Assistant Professor of Aerospace and Systems Engineering. Lecture Notes for MECH 699, Spaceflight Dynamics. School of Engineering, Air Force Institute of Technology, Wright-Patterson AFB OH, 1992.
8. Hall, Christopher D., Assistant Professor of Aerospace and Systems Engineering. Lecture Notes for MECH 533, Problems in Spaceflight. School of Engineering, Air Force Institute of Technology, Wright-Patterson AFB OH, 1993.
9. Hartbaum, H., W. Hooker, I. Leliakov, and G. Margulies. "Configuration Selection for Passive Gravity-Gradient Satellites," *NASA SP-107 — Symposium on Passive Gravity-Gradient Stabilization*. Washington DC: National Aeronautics and Space Administration, 1966.
10. Hartbaum, Helmut K. "Station Keeping for Passive Gravity-Gradient Satellites," *NASA SP-107 — Symposium on Passive Gravity-Gradient Stabilization*. Washington DC: National Aeronautics and Space Administration, 1966.
11. Hodge, W.F. "Influence of Solar Radiation Pressure on Orbital Eccentricity of a Gravity-Gradient-Oriented Lenticular Satellite," *NASA SP-107 — Symposium on Passive Gravity-Gradient Stabilization*. Washington DC: National Aeronautics and Space Administration, 1966.
12. Hoyle, Fred. *Astronomy and Cosmology - A Modern Course*. San Francisco: W.H. Freeman and Co., 1975.
13. Hughes, Peter C. *Spacecraft Attitude Dynamics*. New York: John Wiley and Sons, 1986.
14. Kane, T.R. and P.W. Likins, "Comment on Equilibrium Orientations of Gravity-Gradient Satellites," *AIAA Journal*, 2: 1357 (1964).

15. Kelley, David H. Mission Director and Deputy Chief, Advanced Plans Division, Secretary of the Air Force Office of Special Projects. Personal interview. Wright-Patterson AFB OH, 1993.
16. Kelso, T.S. Assistant Professor of Space Operations. Personal interview. School of Engineering, Air Force Institute of Technology, Wright-Patterson AFB OH, 1993.
17. Likins, P.W. and R.E. Roberson. "Uniqueness of Equilibrium Attitudes for Earth-Pointing Satellites," *The Journal of the Astronautical Sciences*, 13: 87-88 (March-April 1966).
18. Mancini, Armando and Robert A. Schow, Jr. "Satellite Gravity-Gradient Applications for Geodetic Determinations," *NASA SP-107 — Symposium on Passive Gravity-Gradient Stabilization*. Washington DC: National Aeronautics and Space Administration, 1966.
19. Marandi, S.R. and V.J. Modi. "Use of the Energy Equation in Determining Stability Bounds of Asymmetric Satellites," *The Journal of the Astronautical Sciences*, 37: 121-143 (April-June 1989).
20. Meirovitch, Leonard. *Methods of Analytical Dynamics*. New York: McGraw-Hill, 1970.
21. Meirovitch, Leonard. "On the Effect of Higher-Order Inertia Integrals on the Attitude Stability of Earth-Pointing Satellites," *The Journal of the Astronautical Sciences*, 15: 14-18 (January-February 1968).
22. Michelson, I. "Equilibrium Orientations of a Gravity-Gradient Satellites," *AIAA Journal*, 1: 493 (1963).
23. Mobley, Frederick F. and Robert E. Fischell. "Orbital Results from Gravity-Gradient-Stabilized Satellites," *NASA SP-107 — Symposium on Passive Gravity-Gradient Stabilization*. Washington DC: National Aeronautics and Space Administration, 1966.
24. *NASA SP-107 — Symposium on Passive Gravity-Gradient Stabilization*. Washington DC: National Aeronautics and Space Administration, 1966.
25. Ortega, J.M. "The Newton-Kantorovich Theorem," *American Mathematical Monthly*, 75: 658-660 (1968).
26. Ortega, J.M. and W.C. Rheinboldt. *Iterative Solution of Nonlinear Equations in Several Variables*. New York: Academic Press, 1970.
27. Press, William H., Brian P. Flannery, Saul A. Teukolsky, William T. Vetterling. *Numerical Recipes — The Art of Scientific Computing*. New York: Cambridge University Press, 1986.
28. *Proceedings of the Symposium on Gravity Gradient Attitude Stabilization 3-5 December 1968*. Alexandria VA: Defense Technical Information Center, 1969.
29. Rice, John M. *Numerical Methods, Software, and Analysis*. New York: McGraw Hill, 1983.
30. Rimrott, F.P.J. "Storable Tubular Extendable Member - A Unique Machine Element," *Machine Design*, 37: 156-165 (December 9, 1965).
31. Rimrott, F.P.J. *Introductory Attitude Dynamics*. New York: Springer-Verlag, 1989.

32. Roberson, Robert E. "Circular Orbits of Non-Infinitesimal Material Bodies in Inverse Square Fields," *The Journal of the Astronautical Sciences*, 15: 80-84 (March-April 1968).
33. Sarichev, V.A. "Asymptotically Stable Rotational Motions of a Satellite," *Peaceful Uses of Automation in Outer Space - Proceedings of the First IFAC Symposium on Automatic Control in the Peaceful Uses of Space* held June 21-24, 1965 in Stavanger, Norway, edited by John A. Aseltine. 277-285. New York: Plenum Press, 1966.
34. Seaman, Calvin. Principal Investigator for HST EVA Developmental Test Objective 671. Personal interview. NASA Johnson Space Center, 18 August 1993.
35. Seydel, R. *From Equilibrium to Chaos: Practical Bifurcation and Stability Analysis*. New York: Elsevier Science Publishing Co., 1988.
36. Simo, J.C, D. Lewis, and J.E. Marsden, "Stability of Relative Equilibria: Part I. The Reduced Energy-Momentum Method," *Archive for the Rational Mechanics and Analysis*, 115: 15-60 (1991).
37. Scott, William B. "Corrective Optics for Hubble On Track for Launch Next Year," *Aviation Week and Space Technology*: 135 (24 February 1992).
38. Thomson, William T. "Spin Stabilization of Attitude Against Gravity Torque," *The Journal of the Astronautical Sciences*, 9: 31-33 (Spring 1962).
39. Tinling, Bruce E. and Vernon K. Merrick. "Exploitation of Inertial Coupling in Passive Gravity-Gradient-Stabilized Satellites," *Journal of Spacecraft and Rockets*, 1: 381-387 (July-August 1964).
40. Wang, Li-Sheng. *Geometry, Dynamics, and Control of Coupled Systems*. Ann Arbor MI: University Microfilms International, 1990.
41. Wang, Li-Sheng, P.S. Krishnaprasad, and J.H. Maddocks. "Hamiltonian Dynamics of a Rigid Body in a Central Gravitational Field," *Celestial Mechanics and Dynamical Astronomy*, 50: 349-386 (1991).
42. Wang, Li-Sheng, J.H. Maddocks, and P.S. Krishnaprasad. "Steady Rigid-Body Motions in a Central Gravitational Field," *The Journal of the Astronautical Sciences*, 40: 449-478 (October-December 1992).
43. Watson, DeLamar M. "Energy Approach to Passive Gravity-Gradient Satellite Capture Problem," *NASA SP-107 — Symposium on Passive Gravity-Gradient Stabilization*. Washington DC: National Aeronautics and Space Administration, 1966.
44. Watson, Layne T. "Numerically Linear Algebra Aspects of Globally Convergent Homotopy Methods," *SIAM Review*, 28: 529-543 (December 1986).
45. Wertz, James R. *Spacecraft Attitude Determination and Control*. Boston: Reidel, 1985.
46. Wiesel, William E. *Spaceflight Dynamics*. New York: McGraw Hill, 1989.
47. Wiggins, Lyle E. "Relative Magnitudes of the Space-Environment Torques on a Satellite," *AIAA Journal*, 2: 770-771 (1964).
48. Wittenburg, J. and L. Lilov. "Relative Equilibrium Positions and Their Stability for a Multi-Body Satellite in a Circular Orbit," *Ingenieur Archiv*, 44: 269-279 (1975).

49. Zimmerman, Benjamin G. "Study of Gravity-Gradient Experiment of Application Technology Satellite," *NASA SP-107 — Symposium on Passive Gravity-Gradient Stabilization*. Washington DC: National Aeronautics and Space Administration, 1966.

Vita

Captain Cynthia A. (Broderick) Provost was born in Poughkeepsie, New York on May 24, 1966. She attended schools in Connecticut, Colorado, and Georgia before graduating in 1984 from Union High School, Tulsa, Oklahoma. After earning a Bachelor of Science degree in Aerospace Engineering from the University of Notre Dame, she was commissioned through ROTC on December 16, 1988. During her first assignment as a Space Surveillance Engineer for the former Foreign Technology Division (FTD), she began taking part-time classes at the Air Force Institute of Technology (AFIT) and also met Captain Rob Provost, an intelligence officer also at FTD. In July of 1992, then-Lieutenant Broderick enrolled as a full-time student in the 1993 class of Astronautical Engineering at AFIT. While at AFIT, she married Rob and earned an additional Masters Degree in Space Operations. Following her graduation from AFIT, she was assigned to the 2nd Space Operations Squadron at Falcon AFB, CO. She is a member of the American Institute of Aeronautics and Astronautics, Tau Beta Pi, and Sigma Gamma Tau.

Permanent address: 49 Flower Road
Hopewell Junction, New York 12533

REPORT DOCUMENTATION PAGE

Form Approved
OMB No. 0704-0188

Public reporting burden for this collection of information is estimated to average 1 hour per response, including the time for reviewing instructions, searching existing data sources, gathering and maintaining the data needed, and completing and reviewing the collection of information. Send comments regarding this burden estimate or any other aspect of this collection of information, including suggestions for reducing this burden, to Washington Headquarters Services, Directorate for Information Operations and Reports, 1215 Jefferson Davis Highway, Suite 1204, Arlington, VA 22202-4302, and to the Office of Management and Budget, Paperwork Reduction Project (0704-0188), Washington, DC 20503.

1. AGENCY USE ONLY (Leave blank)		2. REPORT DATE December 1993		3. REPORT TYPE AND DATES COVERED Master's Thesis	
4. TITLE AND SUBTITLE STEADY MOTIONS OF RIGID BODY SATELLITES IN A CENTRAL GRAVITATIONAL FIELD				5. FUNDING NUMBERS	
6. AUTHOR(S) Cynthia A. Provost, Captain, USAF					
7. PERFORMING ORGANIZATION NAME(S) AND ADDRESS(ES) Air Force Institute of Technology, WPAFB OH 45433-6583				8. PERFORMING ORGANIZATION REPORT NUMBER AFIT/GA/ENY/93D-8	
9. SPONSORING / MONITORING AGENCY NAME(S) AND ADDRESS(ES) Dr. Arje Nachman AFOSR/NM Bolling AFB, DC 20332				10. SPONSORING / MONITORING AGENCY REPORT NUMBER	
11. SUPPLEMENTARY NOTES					
12a. DISTRIBUTION / AVAILABILITY STATEMENT Approved for public release; distribution unlimited				12b. DISTRIBUTION CODE	
13. ABSTRACT (Maximum 200 words) Numerous studies have been conducted on equilibrium orientations of objects moving under the influence of a central gravitational field. The results of many of these studies conclude that equilibrium conditions exist only when one of the principal axes coincides with the radius vector. Furthermore, these results assume that the center of force is located within the orbit plane, thereby tracing a great circle orbit. While these previous works have approximated the gravitational potential, this study examines relative equilibria obtained by retaining an exact expression for the potential of a spherical primary body, as shown in a recent paper by Wang, Maddocks, and Krishnaprasad. The exact dynamic equations for the motion of a finite rigid body in an inverse square gravitational force field are investigated. Only circular orbits for a specific satellite model consisting of six masses connected by three massless rigid rods are considered. The system dynamics are comprised of seven nonlinear equations, which were numerically solved on a Cray computer. The existence of equilibrium orientations which establish non-great circle orbits was verified and other interesting results were noted. The operational significance of these results was also examined.					
14. SUBJECT TERMS Equilibrium, Gravity-Gradient, Continuation, Artificial Satellites, AUTO, Gravitational Fields, Satellite Attitude, Numerical Analysis, Newton-Raphson				15. NUMBER OF PAGES 89	
				16. PRICE CODE	
17. SECURITY CLASSIFICATION OF REPORT Unclassified	18. SECURITY CLASSIFICATION OF THIS PAGE Unclassified	19. SECURITY CLASSIFICATION OF ABSTRACT Unclassified	20. LIMITATION OF ABSTRACT UL		